

High-resolution drought simulations and comparison to soil moisture observations in Germany

Friedrich Boeing¹, Oldrich Rakovec^{1,2}, Rohini Kumar¹, Luis Samaniego¹, Martin Schrön³, Anke Hildebrandt¹, Corinna Rebmann¹, Stephan Thober¹, Sebastian Müller¹, Steffen Zacharias³, Heye Bogena⁴, Katrin Schneider⁵, Ralf Kiese⁵, and Andreas Marx¹

¹Helmholtz Centre for Environmental Research – UFZ, Department Computational Hydrosystems, Permoserstraße 15, 04318 Leipzig, Germany

²Faculty of Environmental Sciences, Czech University of Life Sciences Prague, Praha-Suchbát 16500, Czech Republic

³Helmholtz Centre for Environmental Research – UFZ, Department Monitoring and Exploration Technologies, Permoserstraße 15, 04318 Leipzig, Germany

⁴Forschungszentrum Jülich GmbH, Agrosphere Institute (IBG-3), Germany

⁵Karlsruhe Institute of Technology, IMK-IFU, Ecosystem Matter Fluxes, Kreuzeckbahnstr. 19, 82467 Garmisch-Partenkirchen, Germany

Correspondence: Friedrich Boeing (friedrich.boeing@ufz.de)

Abstract. ~~The Germany's~~ 2018-2020 consecutive drought events ~~in Germany~~ resulted in impacts related with several sectors such as agriculture, forestry, water management, ~~industry, energy production~~energy production, and transport. ~~A major national operational drought information system is the German Drought Monitor~~ The key to preparedness for extreme drought events are high-resolution information systems. This study evaluates the new setup of the one-kilometre German drought monitor (GDM), launched in 2014. It provides which is based on the daily soil moisture (SM) ~~simulated with simulations from~~ the mesoscale hydrological model (mHM)~~and its related soil moisture index at a spatial resolution of 4×4 km². Key to preparedness for extreme drought events are high-resolution information systems. The release of the new soil map BUEK200 allowed to increase the model resolution to ≈1.2×1.2 km², which is used in the second version of the GDM. In this paper, we explore the ability to provide drought information on the one-kilometer scale in Germany. Therefore, we compare simulated SM dynamics using homogenized and deseasonalized SM observations to evaluate the high-resolution drought simulations of the GDM. These SM observations are obtained. The simulated SM is compared against a set of diverse observations from single profile measurements, spatially distributed sensor networks, cosmic-ray neutron stations and lysimeters at 40 sites in Germany. The results Results show that the agreement of simulated and observed SM dynamics is especially high in the ~~vegetation~~vegetative active period (0.84 median correlation R) and lower in winter (0.59 median R). Lower agreement in winter results from methodological uncertainties in simulations as well as in observations. Moderate but significant improvements between the ~~first and second GDM version to observed SM were found in correlations for older (coarser 4km resolution) setup and the present (≈1.2km resolution) GDM is found in~~ autumn (+0.07 median R) and winter (+0.12 median R). The ~~annual drought intensity ranking and the spatial structure of drought events over the past 69 years is comparable for the two GDM versions. However, the~~ higher resolution of the second GDM version allows for a much more detailed representation of the spatial variability of SM, which is particularly beneficial for local risk assessments. Furthermore, the results underline that~~

nationwide drought information systems depend both on appropriate simulations of the water cycle and a broad, high-quality observational soil moisture database.

1 Introduction

The extreme drought events since 2018 in Germany lead to multi-sectoral impacts (Madruga de Brito et al., 2020) and increased stakeholder awareness. Moreover, recent studies emphasized that extreme soil moisture drought events will be more likely and more severe in Central Europe under future warming scenarios (Samaniego et al., 2018; Grillakis, 2019). The singularity of the 2018/19 drought within observational records in terms of consecutive multiyear water deficits was confirmed for Germany and Central Europe (Boergens et al., 2020; Hari et al., 2020)(Boergens et al., 2020; Hari et al., 2020; Rakovec et al., 2022). With these prospects comes an increased need for state-of-the-art information on droughts as a basis for precisely assessing the uniqueness and potential impacts of drought events from local to continental scales.

In recent years, several national and supranational drought monitoring systems were developed. The German Drought Monitor (GDM) was first introduced in 2014 as an information platform for agricultural droughts in Germany under www.ufz.de/droughtmonitor and is operationally updated daily (Zink et al., 2016). Core of the GDM is simulated soil moisture using the open-source mesoscale hydrological model (mHM, (Samaniego et al., 2010; Kumar et al., 2013)). The GDM provides a near real-time status of soil moisture and drought in Germany with a time lag of one day due to meteorological data availability. Information on the drought status is provided for the uppermost soil layer (25 cm) and total soil column (depth variable, depending on soil map) by calculating the Soil Moisture Index (SMI) (Samaniego et al., 2013) and Plant Available Water (PAW). With its use in national and federal state agencies, around 2200 media contributions in the year 2020 and more than four Million website views since 2018, it proved its important role as a drought information tool in Germany. Feedback and requests showed that the GDM is both used by interested public and practitioners as well as media and politics to obtain up-to-date drought information. A crucial aspect for the optimal use of scientific, environmental data from a practitioners point of view is the applicability to local purposes. Targeted stakeholder interviews within the EDgE project <http://edge.climate.copernicus.eu> and in Climalert (<http://climalert.eu/>) with a core stakeholder group of 15 farmers in Central Germany supported this need. So far, hydrological models that were applied at national or supranational level in operational drought services were mostly run on "relative" low spatial resolutions, e.g. grid cell size $5 \times 5 \text{ km}^2$ in the European drought observatory (EDO) (Sepulcre-Canto et al., 2012) or $4 \times 4 \text{ km}^2$ in the GDM (Zink et al., 2017). The spatial resolution was mainly restricted due to input data availability, such as the soil map BUEK1000 (spatial resolution 1:1,000,000) for Germany.

Recently, an updated version of the nationwide German soil database (BGR, 2020) was published at 25 times higher resolution that enabled to take a step forward to hydrological modelling at much higher spatial resolution ($\approx 1.2 \times 1.2 \text{ km}^2$, ≈ 11 fold increase to prior GDM version). Nevertheless, it was not clear how the quality of the soil moisture simulations would change at higher spatial resolution. In contrast to other environmental variables, for instance, air temperature, it is much more challenging to aggregate soil moisture to a larger scale due to its highly heterogeneous nature and measurement uncertainties (Western et al., 2004; Bogaen et al., 2010; Rosenbaum et al., 2012). Simulated soil moisture derived from hydrological

models is the prime alternative to observed soil moisture and widely employed to estimate soil moisture on regional to global scales (Keyantash and Dracup, 2002). Nevertheless, simulations face methodological uncertainties as well (Marx et al., 2018, e.g.). Cammalleri et al. (2015) investigated the use of multiple hydrological models for drought monitoring in Europe using SM anomalies and drought classification metrics and found that including several hydrological models improved the overall performance. Furthermore, hydrological models are typically calibrated based on streamflow since it represents the integral hydrological catchment response. Yet, besides validating the modelled streamflow itself, a clear need to thoroughly evaluate other water cycle components that are not used for constraining the model parameters emerges. Ideally, such validations require observations of the variable of interest that a) span the same spatial scales as the model and extend across different climate regimes within the study area and b) span long temporal scales, which would allow them to be termed “representative”. Therefore, optimal drought monitoring systems over large areas can only be built up using of the best available observation data in combination with a smart simulation system.

Enormous efforts have been and are being made to build up environmental observation networks from regional to global scales. Within global environmental monitoring networks such as FLUXNET that focuses on measuring ecosystem carbon fluxes (Baldocchi et al., 2001), soil moisture is usually measured in multiple depths at single profiles. However, extensive validations of simulated soil moisture from hydrological models are hampered by the limited spatial representativeness of point-scale sensors and hence require novel measurement approaches to bridge the scale gap between local observations and model resolutions. Measurements that capture the spatial structure of soil moisture at larger scales are expensive and time-consuming. For this reason they are rare and only applicable in comparatively small catchments of a few tens of hectares (Bogena et al., 2010). In Germany, the infrastructure of Terrestrial Environmental Observatories (TERENO) has been established since 2008 to build up a nationwide long-term monitoring network where one of the focuses is on hydrological variables (Zacharias et al., 2011; Bogena, 2016). Many of those sites were equipped with spatially distributed measurements of soil moisture networks (SDM, Bogena et al., 2010) and Cosmic-Ray Neutron Sensors (CRNS, Zreda et al., 2012; Andreasen et al., 2017; Schrön et al., 2018)). CRNS detectors count neutrons of the natural cosmic-ray background radiation as a proxy for soil water content (Desilets et al., 2010; Köhli et al., 2021). The integral measurement footprint covers areas of 300–600 m diameter and depths of 15–70 cm, both increasing for dryer conditions (Köhli et al., 2015; Schrön et al., 2017). The method has emerged as a reliable technique to continuously monitor root-zone soil moisture at the field scale (Bogena et al., 2015; Andreasen et al., 2017) and has been used recently for the validation of land surface and hydrological models (Han et al., 2016; Iwema et al., 2017; Dimitrova-Petrova et al., 2020).

On the other hand, satellite-based soil moisture data benefits from spatial coverage at the km scale. Still, the shallow penetration of the signal in the upper few centimeters of the soil is a significant constraint. While those signals also depend on the surface condition, vegetation density and microwave frequencies, these products themselves require ground-based soil moisture observations for validation (Peng et al., 2021). To evaluate the performance of the drought monitor model, the time series of SDM and CRNS observations at the TERENO sites appear to be better suited in terms of long-term continuity and root-zone representation. In particular, the data covers recent wet (e.g. 2017) and dry (e.g. 2015, 2018-2020) years, including extreme drought conditions.

Here, we evaluate soil moisture simulations at the one and four kilometer scale simulated from mHM against an unprece-
90 dented compilation of soil moisture observations from 40 locations across Germany. A wide range of climatic conditions and
vegetation types is covered. Specifically, the study aims at two objectives. Firstly, how well do high-resolution German-wide
soil moisture simulations capture the SM dynamics in observed soil moisture that constitute the basis for the near real-time soil
moisture drought monitoring system? Emphasis is given to distinguish between different soil moisture measurement techniques
due to their relevance for interpreting the evaluation results. Secondly, can the simulations with higher spatial resolved soil in-
95 put data be provided with a consistent quality of soil moisture estimates? Higher resolution does not automatically increase the
model performance but may even worsen the quality of the simulation results. To assess this effect, the low-resolution model
setup GDM-v1-2016 as well as the one kilometer setup GDM-v2-2021 are compared against multi-method soil moisture obser-
vations. Furthermore, drought characteristics estimated with both model setups are compared using annual drought intensities
over the last 69 years (1952-2020).

100 2 Methods and Datasets

2.1 The mesoscale hydrological model (mHM)

The mesoscale hydrological model is a grid-based spatially distributed hydrologic model forced with daily precipitation,
temperature and potential evapotranspiration PET. It accounts for major hydrologic processes such as snow generation and
snowmelt, canopy interception, soil infiltration, ET, deep percolation, baseflow generation, and surface runoff routing. The
105 open-source model code is available in git and is under active development and maintenance (<https://git.ufz.de/mhm/mhm>).
The model uses three distinct levels to organize the modelling procedures: level 0 (L0) for input data of the sub-grid physical
basin characteristics, level 1 (L1) for the realization of the integrated hydrological processes and level 2 (L2) for specification
of meteorological forcing inputs. An unique component of mHM is the Multiscale Parameter Regionalization (MPR) tech-
nique (Samaniego et al., 2010) that allows inferring spatial variability of the required model parameters seamlessly on various
110 modelling scales. One of the distinguishing aspects of the MPR approach compared to other regionalization techniques is to
deliver a quasi scale-invariant model performance across modelling scales and improve the transferability of model parameters
to ungauged basins (Kumar et al., 2013; Rakovec et al., 2016; Samaniego et al., 2017). [The mHM was applied and evaluated
in different climatological regions e.g. Europe \(Thober et al., 2015; Rakovec et al., 2016\), West Africa \(Dembélé et al., 2020\)
, India \(Saha et al., 2021\) and US \(Livneh et al., 2015; Rakovec et al., 2019\).](#) Within the MPR technique, the subgrid physical
115 basin characteristics at L0 are linked to model parameters through transfer functions and a set of global parameters and subse-
quently upscaled to generate effective parameters at L1. The aggregation has based a set of upscaling rules (e.g. arithmetic or
harmonic mean) following, e.g. flux conservation schemes (Samaniego et al., 2010).

A general overview on the model processes and parameterization can be obtained from Samaniego et al. (2010) and Kumar
et al. (2013). In the following only the soil moisture component of mHM is described due to its relevance for this study. The
120 incoming precipitation and snowmelt are partitioned into root-zone soil moisture and runoff components, depending on the
degree of soil saturation, using a power function similar to the well-known HBV model (Samaniego et al., 2010). The degree

of non-linearity depends on underlying vegetation and soil characteristics following the MPR framework (Samaniego et al., 2010; Kumar et al., 2013). The evapotranspiration from soil layers is estimated as a fraction of the potential evapotranspiration depending on the soil moisture stress and the fraction of vegetation roots present in each layer (Samaniego et al., 2010). The moisture stress function depends on the specification of soil-water content at a permanent wilting point, critical and saturation levels, which are determined using a set of pedo-transfer functions estimated within the MPR framework (Livneh et al., 2015; Zacharias and Wessolek, 2007).

2.2 Model setups at 4×4 km² and 1.2×1.2 km² spatial resolution

The new setup GDM-v2-2021 used in the GDM version 2 includes several changes compared to the older model setup GDM-v1-2016. The main features of the two mHM model setups that are used in the analysis are described in Table 1. While the GDM-v1-2016 uses the mHM model version 5.6, in GDM-v2-2021 the mHM model was updated to version 5.10 (see <https://github.com/mhm-ufz>). ~~However, the~~ The implemented changes in the mHM model did not change the hydrological process representations related to soil moisture that were used in the simulations here. Between the setups GDM-v1-2016 and GDM-v2-2021, the projection system was changed from the projected coordinate system Gauss-Krueger 4 (EPSG:31468) to the World Geodetic coordinate System (EPSG:4326). While the lengths of the grid cells in the GDM-v1-2016 setup were fixed on 4×4km² (L1 level), the grid cell sizes in the GDM-v2-2021 setup are measured in degree, where the grid cell length varies with latitude with a decreasing grid cell length in east/west direction from 1.23 km at 45° N latitude (south of Germany) decreasing to 0.98 km at 55.5° N latitude (north of Germany) and a constant grid cell length of 1.7 km in north/south direction.

Table 1. Main features of the model setups GDM-v1-2016 and GDM-v2-2021. Core of the setups is the mesoscale hydrological model mHM. Vertical discretization of soil layers in the hydrological model mHM and projection system are denoted. In the spatial model resolution the Level 0 (L0) describes subgrid variability of relevant basins characteristics. Level 1 (L1) and Level 2 (L2) describe dominant hydrological processes and meteorological forcings, respectively. Underlying datasets for soil as well as land use and geology used as model inputs for mHM on L0 model resolution are stated.

Setup	spatial model resolution	soil dataset	vertical soil discretization	projection	landuse dataset	geology dataset
GDM-v2-2021	L1 and L2: 0.01562×0.01562° eq. ~1.2×1.2km ² L0: 0.001953125× 0.001953125°	BUEK200	4 layers: 0–5 cm 5–25 cm 25–60 cm 60 - variable	Latlon (EPSG:4326)	GLOBCOVER	GLIM
GDM-v1-2016	L1 and L2: 4×4km ² L0: 100×100m ²	BUEK1000	3 layers: 0–5 cm 5–25 cm 25 - variable	Gauss Krüger-4 (EPSG:31468)	CORINE	HUEK200

Soil physical properties on texture (sand and clay fraction) and mineral bulk density are derived from national digital soil maps provided by the BGR (Federal Institute for Geosciences and Natural Resources). The BUEK200 dataset (BGR, 2020) used in the GDM-v2-2021 setup substantially increased the mapping resolution compared to the BUEK1000 dataset (BGR, 1998) used in the GDM-v1-2016 setup (scale 1:1 000 000 to 1:200 000). At the time of the creation of this study, the database version of BUEK200 was V0.5. Figure 1 shows the depth averaged clay contents exemplary for a region in Central Germany where soil moisture observations ~~are located~~ that were used in the analysis are located. The soil maps aim to represent the local soil composition by identifying patterns of similar soils. The base mapping unit of the soil maps are soil series, which can include multiple soil profiles that associate soils with similar compositions. For the derivation of the BUEK200 dataset the index soils, meaning the dominant soil in a soil series, were considered.

The soil depths in mHM are discretized into an upper soil layer for 0–25 cm, including a top layer 0–5 cm and the remaining depth of the soil profile. In the GDM-v2-2021 setup an additional layer for 25–60 cm was added due to stakeholder feedback mainly from the agricultural sector. The rooting depth is set to 30 cm in both model setups. Landuse datasets used in the model setups GDM-v1-2016 and GDM-v2-2021 are CORINE (EEA, 2009) and GLOBCOVER (ESA, 2009), respectively. Hydro-geological input data was derived from the HUEK200 (BGR, 2009) and GLIM (Hartmann, Jörg and Moosdorf, Nils, 2012) databases, respectively. Digital elevation models were derived from BKG (2010) and USGS (2017), respectively. The changes in landuse and geology datasets can influence the simulations, yet play a minor role for the soil moisture simulations compared to the change in the soil dataset, because changes of landuse data are in subgrid scale (resolution GLOBCOVER 300m, CORINE <100m) and no direct feedback of from saturated “groundwater” storage to soil moisture storage is implemented in mHM.

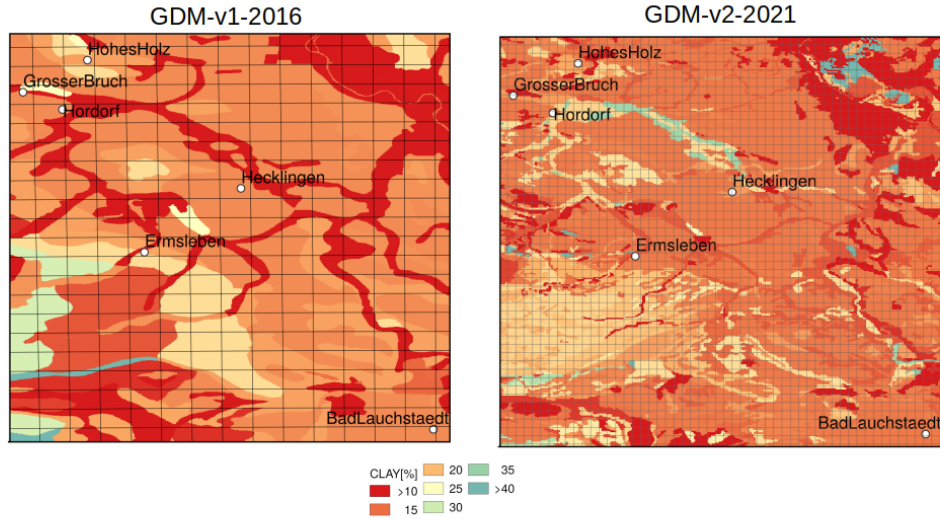


Figure 1. Average over soil column for the derived soil physical properties clay [%] of BUEK1000 soil dataset used in the GDM- v1-2016 model setup (left panel) versus BUEK200 soil dataset used in the GDM-v2-2021 model setup (right panel). The grid shows the respective modelling resolution L1 at which the hydrological processes are simulated (see table 1). Both setups are projected in WGS 84 (EPSG:4326).

2.2.1 Meteorological input data

Precipitation, as well as minimum, maximum and average air temperature, are interpolated on a daily timescale based on meteorological station data from the German Weather Service DWD using external drift kriging (EDK) with elevation as the drift variable. The [meteorological station data is subject to extensive quality controls \(Kaspar et al., 2013\). Additionally, quality controls are implemented in the preprocessing steps of the interpolation routine e.g. checking plausible variable range. The interpolation method and variogram parameter estimation for Germany are described and evaluated in detail in Zink et al. \(2017\) including cross-validation metrics and comparison to the comparable REGNIE gridded dataset by the German Weather Service \(Rauthe et al., 2013\)](#). Potential Evaporation (PET) is calculated using the [Hargreaves-Samani](#) [Hargreaves-Samani](#) Method (Hargreaves and Samani, 1985) that is based on the interpolated temperature fields (average, minimum, and maximum), where (potential) extraterrestrial radiation is computed depending on the latitude of the location and day of the year.

2.2.2 Multibasin Model Calibrations

The unknown parameters of the mHM model setup GDM-v2-2021 were calibrated against observed discharge using the Kling-Gupta efficiency (KGE; Gupta et al., 2009) as the objective function. The parameter optimization was conducted using the Dynamically Dimensioned Search (DDS; Tolson and Shoemaker, 2007) algorithm (1 000 iterations), which underwent detailed scrutiny. In a first step, 200 parameter sets were obtained using a multi-basin/domain-wide joint basin calibration strategy, in

which a subset of 6 basins was randomly selected (out of 201 total number of basins) and then jointly calibrated during a common period of 1990-2005 ([See Table S1 in the Supplements](#)). In the second step, all 200 parameter sets were evaluated against the full ensemble of the 201 basins during an extended period of 1986–2005 (with a warming period of 5 years). The single unique parameter set with the best performance in terms of the median daily KGE over 201 basins was selected and used for the consequent analysis ([See Table S2 in the Supplements](#)). This updated approach is based on the earlier calibrations of the GDM-v1-2016 setup (Zink et al., 2017) in which the Nash–Sutcliffe efficiency instead of the KGE was applied and individual single-basin instead of the multi-basin calibrations were carried out as input to the model cross-evaluation at locations that were not used for model calibration. [Previous works also focused on multibasin calibrations of mHM in other regions, such as Mizukami et al. \(2017\); Rakovec et al. \(2019\).](#) The model performance of the best cross-evaluated parameters of the GDM-v2-2021 based on daily streamflow from 201 catchments in Germany yielded a median performance of 0.761 KGE (see Fig. A1).

2.3 Soil Moisture Observations

The soil moisture observations used to conduct the model evaluations were gathered from the environmental observation networks TERENO (Zacharias et al., 2011) and FLUXNET (FLUXNET2015 Dataset (Pastorello et al., 2020)) as well as from the Cunnersdorf site operated by the DWD (German Weather Service). In total, soil moisture data from 40 locations were compiled and processed for the analysis (see Fig. 1). Even though it is not feasible to establish an evenly distributed grid of SM measurements on a national level (Vereecken et al., 2008), the available locations cover a wide range of climatic and vegetation conditions in Germany. Four of the sites have multiple measurement methods available (total number (n)= 46), which allows comparing the evaluations between the measurement methods at single sites.

In total, we analyzed 24 grassland, 9 crop, 6 forest and one site with a forest clearing. The elevation ranges from 4 to 1252 meters [asl.a.s.l.](#), and the long-term yearly precipitation sums range from below 500 mm to more than 1500 mm. [Time series lengths of the observations are between 2.8 and 17.8 years with a median \(mean\) of 6.5 \(6.7\) years.](#) A detailed overview of the location characteristics is shown in Table 3. The data comprises four different soil moisture measurement methods explained in more detail in the following.

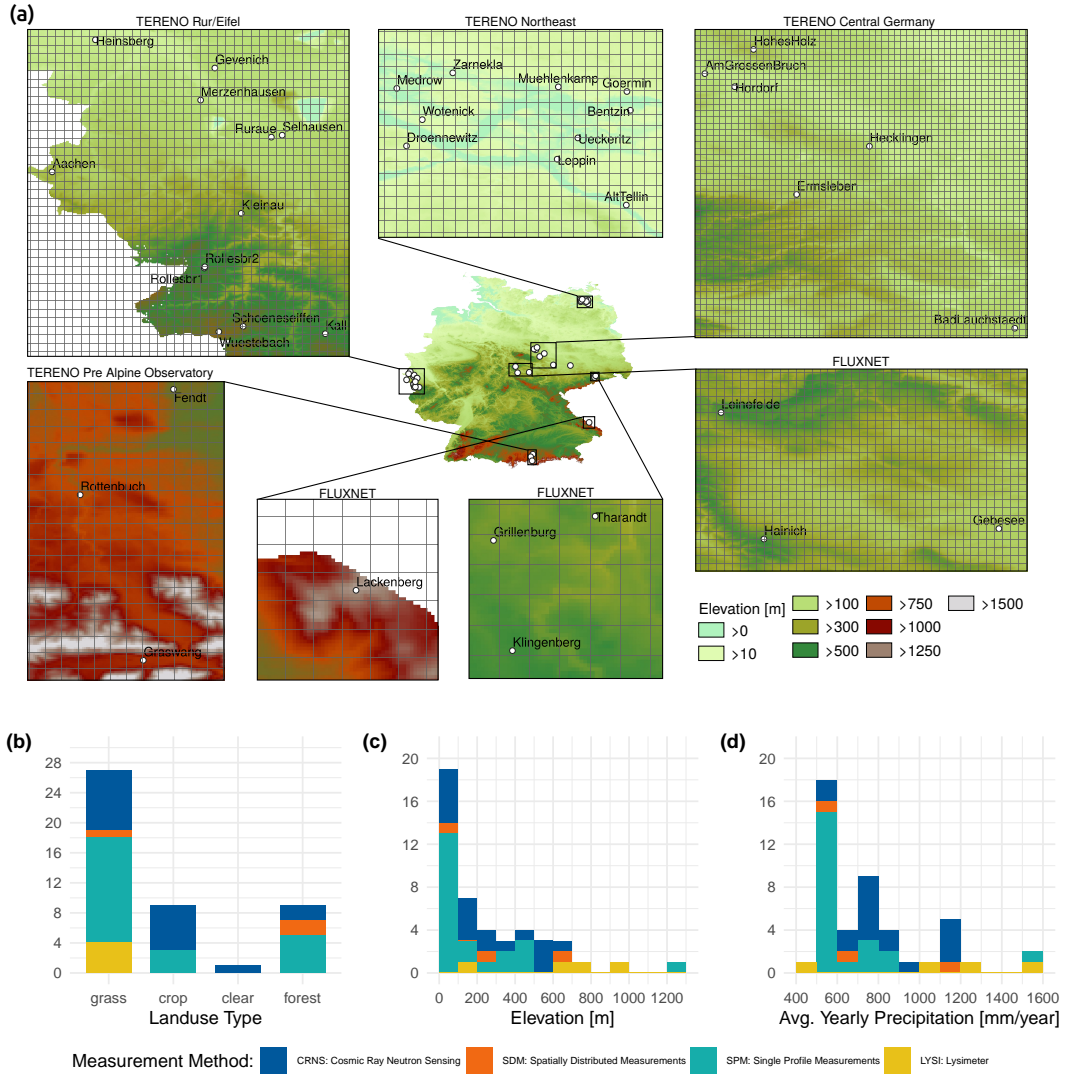


Figure 2. Soil moisture observations of 40 locations distributed over Germany were used in the soil moisture evaluations of the GDM-v2-2021 and GDM-v1-2016 model setups. The subplots zoom to the different experimental sites in Germany, representing different climate gradients in Germany. The maps show the digital elevation model on the hydrological subgrid variability resolution L0 of the mHM model in the GDM-v2-2021 setup ($0.001953125^\circ \times 0.001953125^\circ$). The grid corresponds to the modelling resolution L1 in the GDM-v2-2021 setup ($0.01562^\circ \times 0.01562^\circ$ eq. $\sim 1.2 \text{ km} \times 1.2 \text{ km}$) at which the hydrological processes are simulated. Lower panel: distribution of different soil moisture observations depending on landuse type, elevation and average yearly precipitation. Note that some of the 40 locations have multiple soil moisture data sources (n total = 46).

Soil moisture observations from seven FLUXNET and 16 TERENO sites in Germany based on several vertically distributed sensors within one soil profile were used (in the following abbreviated SPM). The sensor depths are described in Table 3. SPM

200 sites used from TERENO-Northeast Observatory are further described in Itzerott et al. (2018a) and Itzerott et al. (2018b). Soil Moisture data from lysimeters are available for four sites from the lysimeter network TERENO-SOILCan (Pütz et al., 2016) at the Bad Lauchstädt experimental site and the TERENO Pre alpine Observatory (PAO) (Kiese et al., 2018). Lysimeters are large vessels containing an undisturbed soil column to allow gravimetric measurements. Since the lysimeter vessels are closed at the bottom, water tension is adjusted to reference measurements at the same depth in the undisturbed soil close to the lysimeter
205 (Pütz et al., 2016; Kiese et al., 2018). In the lysimeters, soil moisture is measured by single sensors in multiple depths. At each SOILCan-site multiple lysimeters are organized in hexagons (Pütz et al., 2016). The number of lysimeters per site are described in Table 3.

For three of the 40 sites (Am Grossen Bruch, Hohes Holz and Wüstebach), spatially distributed measurements (SPM) of soil moisture are available. Multiple sensors are installed in a spatial grid and different depths covering an area of some hundreds
210 of m². For the locations Hohes Holz 39 profiles and Am Grossen Bruch 20 profiles with sensors in multiple depths were used (depths varied slightly between profiles depending on soil property changes). Therefore, they are not denoted explicitly). For the Wüstebach site, 51 profiles with two sensors each at 5, 20, and 50 cm depth were used (Wiekenkamp et al., 2019). The Wüstebach soil moisture measurement network is described in detail in Bogen et al. (2018).

Soil moisture observations derived from Cosmic Ray Neutron Sensing (CRNS) stations were used from 17 sites (see Table 3)
215 of the TERENO observatories (~~Zacharias et al., 2014; Bogen et al., 2018; Schrön et al., 2017~~)([Bogen et al., 2022](#)). The soil albedo component of cosmic-ray neutrons is particularly prone to changes of soil moisture (Desilets et al., 2010; Köhli et al., 2021). However, since neutrons are sensitive to all pools of hydrogen, the measured neutron signal is also affected by biomass (Baatz et al., 2015), intercepted water (Bogen et al., 2013; Schrön et al., 2017), and snow (Schattan et al., 2017) and therefore requires a correction of the measured signal in this respect. In this study, periods of snow cover have been excluded from the
220 CRNS data. Soil moisture from CRNS data has been calculated by standard methods (Desilets et al., 2010; Zreda et al., 2012) and aggregated to daily time steps. This leads to typical statistical uncertainties of less than 3 vol.% (Schrön et al., 2018).

All SM data was checked according to their flagging conventions for doubtful or low-quality values. In some cases, doubtful data was removed manually after personal communication from site maintainers (e.g. for the TERENO PAO lysimeter sites where some sites experienced frost in early 2017). The available SM data in the respective depths was aggregated to weighted
225 vertical averages according to the soil discretization depths in mHM (0–25 cm, 25–60 cm and 0–60 cm). The spatial mean values were calculated for the SDM measurements based on the available sensors.

2.4 Soil moisture data preparation and evaluation metrics

Since the computation of soil moisture drought indices ~~as, e.g. the SMI (Samaniego et al., 2013) including advanced statistical methods as the estimating the~~, including the estimation of soil moisture probability distributions by kernel density estimates,
230 is hampered for the available observed data due to the limited length of observed soil moisture data (<10 years for most locations), the analysis here is based on the comparison of observed to simulated soil moisture. It is widely known that absolute soil moisture values cannot be adequately determined by a regional model (e.g. due to the spatial heterogeneity), yet the hydrological model typically captures the temporal dynamics well (Koster et al., 2009). As drought is defined by the deviation

from normal conditions, soil moisture anomalies are calculated. To preserve the units of volumetric soil moisture [mm/mm]
 235 and the original range of soil moisture dynamics, standardization by dividing standard deviation is not undertaken in this study.
 The anomalies are calculated in two ways. Firstly, the mean of all values in each SM time series is subtracted

$$\theta(anom)_{i,k} = \theta_{i,k} - \bar{\theta} \quad (1)$$

Secondly, the multi-year mean for each day of the year is subtracted to deseasonalize the anomalies. The removal of the
 annual average cycle of SM is necessary for the subsequent drought classification based on percentile thresholds described in
 240 the next section.

$$\theta(deseas - anom)_{i,k} = \theta_{i,k} - \bar{\theta}_i \quad (2)$$

Where i is the calendar day of the year (DOY 1, ..., 365) and k each year available in a data record. To reduce uncertainty in
 the calculation of mean values resulting from heterogeneous and small sample sizes, for each DOY a) a moving window with
 15 days on each side of the day was used to increase sample size b) the multiyear mean of each DOY was calculated based on
 245 the mean of randomly drawing 500 bootstrap samples. The simulated data were masked to the available observed data. Leap
 days were removed before calculating the deseasonalized anomalies.

The evaluation of observed against simulated SM is based on the Spearman rank correlation coefficient (R). The Spearman
 rank correlation coefficient is a non-parametric measure to quantify the strength of a monotonic relationship between two
 variables. The correlations are calculated on whole data records as well as on sub-periods (months, seasons and **vegetation**
 250 **vegetative active** period) to investigate the intra-annual variability in the performance metrics. Paired Wilcoxon signed-rank
 tests were conducted to identify significant changes between the model setups.

2.4.1 Soil Moisture Index Computation and Analysis

Simulated soil moisture by the two model setups is used to compute a Soil Moisture Index (SMI) on the years 1952–2020
 following Samaniego et al. (2013) and Zink et al. (2016) that enables a SM drought analysis based on the long term SM
 255 dataset. The SMI for a given cell and day is estimated as

$$SMI_t = \hat{F}_T(x_t) \quad (3)$$

and it represents the quantile at the soil moisture fraction value x (normalized against the respective saturated soil water
 content).

x_t denotes the simulated monthly soil moisture fraction at a time t and \hat{F}_T is the empirical distribution function estimated
 260 using non-parametric kernel density estimates. The optimal bandwidths are estimated by minimizing a cross-validation error
 estimate. Details regarding the computation of the SMI can be found in Samaniego et al. (2013).

A cell at time t is under drought when $SMI_t < \tau$. Here, τ denotes that the soil water content in this cell is less than the
 values occurring $\tau \times 100\%$ of the time. In this study, τ is set to 0.2 indicating a soil moisture state occurring less than 20%
 of the time. This threshold follows common values for drought classifications that align with typical occurrences of drought

265 impacts, (Svoboda et al., 2002). Drought statistics are calculated on fixed temporal (annual and ~~vegetation~~vegetative active period from April to October) and spatial scales (per grid cell and aggregated for Germany).

The drought intensities (DI) per year are calculated by

$$DI = \frac{1}{dA} \sum_{t_0}^{t_1} \int_A [\tau - SMI_i(t)]_+ \quad (4)$$

270 with area of interest A (here Germany) and duration d ($t_1 - t_0$) in days (annual t_0 Jan 1st to t_1 Dec 31st and ~~vegetation~~vegetative active period t_0 Apr 1st to t_1 Oct 31st). The area under drought is calculated as the percentage of grid cells with $SMI < 0.2$ of the total German surface area (total number of grid cells) averaged over the respective temporal periods. For calculating the cumulative density functions of SM, a common statistical basis of 1951-2015 was used.

3 Results and Discussion

In the following sections, the comparisons of the multi-method soil moisture observations with two hydrological model simulations are presented and discussed to investigate the proposed research objectives. In section 3.1, a comparison of soil moisture observations from different measurement methods to the high-resolution operational model setup GDM-v2-2021 is shown. The setup allows a comparison of observations to the 0–25 cm layer as well as to the additional, deeper soil layer of 25–60 cm. In section 3.2, the differences between the two simulation setups are shown for annual drought intensities during 1952–2020 and compared to soil moisture observations. The two mHM simulations are used in their operational setups, meaning that only 280 data and information available for whole Germany have been used. Additional available information on soils or meteorological measurements at the observation sites has not been incorporated in the simulations.

3.1 Comparison of high resolution simulations against observed SM dynamics

Here, 1.2×1.2 km² simulations in two soil layers (GDM-v2-2021) are compared to SM observations using four different measurement methods: Cosmic Ray Neutron Sensing (CRNS), spatially distributed measurements (SDM), single profile measurements (SPM) and lysimeter (LYSI). In this study, SM anomalies as well as deseasonalized SM anomalies are used. 285

Figure 3 shows the results for three selected locations that contain both ~~r~~-CRNS and SDM measurements for the six-year period 2014–2019. In general, the SM anomalies and deseasonalized data agree well, with small deterioration of correlations in deseasonalized data. Furthermore, observations and simulations compare well in the uppermost 25 cm soil layer and in the deeper layer down to 60 cm depth. The correlation strength between simulations and observations from different measurement techniques is similar for the sites Am Grossen Bruch and Hohes Holz, but deviate more from each other for the Wüstebach site. It is worth noting that different spatial scales are mapped by those measurements. While the SPM (not included here) represents point information, the SDM and CRNS cover an area less than 0.1 km² and the mHM simulations cover an area of ≈ 1.44 km². In general, the day-to-day variability is smaller in simulations than in observations. At the forest sites Wüstebach and Hohes Holz, the day-to-day variability in the CRNS data is higher than in SDM. Several environmental factors other than 295 SM influence the CRNS signals (see method section). While the changing biomass might have a low impact on the signal, it can

introduce a (constant) systematic bias. Since only anomalies are analysed here, the impact of such bias on this (comparative) anomaly analysis should be minimal. Intercepted water on leaves and in the litter layer can be particularly challenging to quantify, especially in forested stations such as Hohes Holz or Wüstebach (Bogena et al., 2013; Schrön et al., 2017). It might lead to stronger dynamics in the CRNS signal during and shortly after rain events, compared to the model output or other observation methods. Additionally, at the Wüstebach site partial deforestation in 2013 modified SM flows that resulted in stronger response to rainfall (Wiekenkamp et al., 2019). Nevertheless, there is no general tendency for lower correlations at forest sites compared to crop and grassland sites (see ~~Fig. 4~~ Figure 4). Crop sites show slightly lower correlations than grassland sites, which is expected since anthropogenic activities (e.g., crop rotation) are not represented in mHM. Correlations display no clear tendency across the range of elevation and precipitation regimes. In general, Figure 4 reveals that the model performances does not systematically depend on site conditions. As well, no trend of deteriorating correlations with length of time series can be detected (see Figure 4 d)).

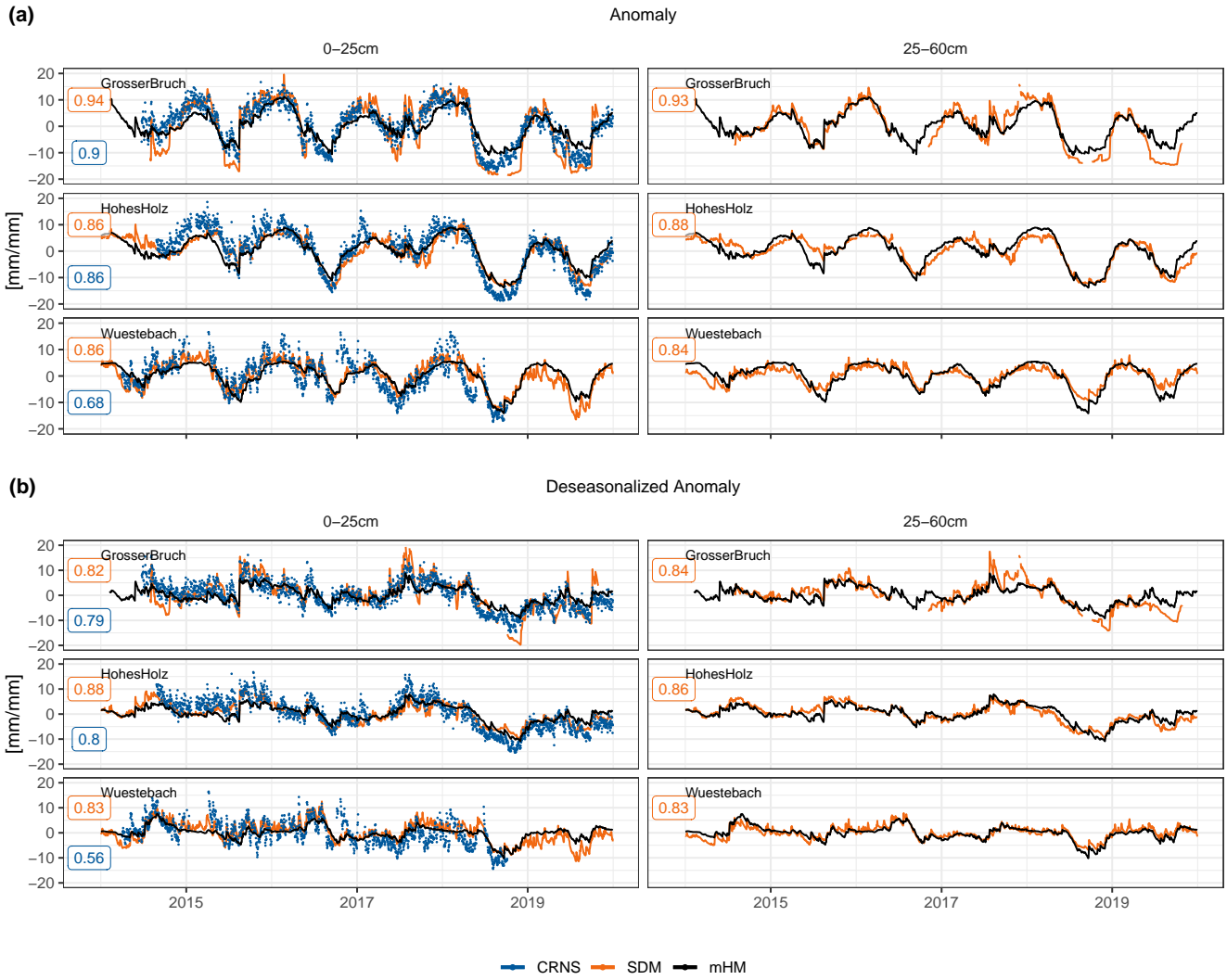


Figure 3. Soil moisture [timeseries-time series](#) for the years [2014–2019](#) for the selected locations Am Grossen Bruch, Hohes Holz and Wüstebach showing SDM and CRNS data against simulated data from mHM in [0–25](#) cm and [25–60](#) cm depth in the GDM-v2-2021 setup. [The Hordorf site also contains both CRNS and SDM measurements, but with much shorter time series length. For visualization the stations with longer time series were selected.](#) Correlation Coefficients are denoted. Upper panel shows anomalies, including seasonality (subtract mean of the whole time series) and lower panels show de-seasonalized anomalies (subtracting multiyear mean for each calendar day) analyzed in this study.

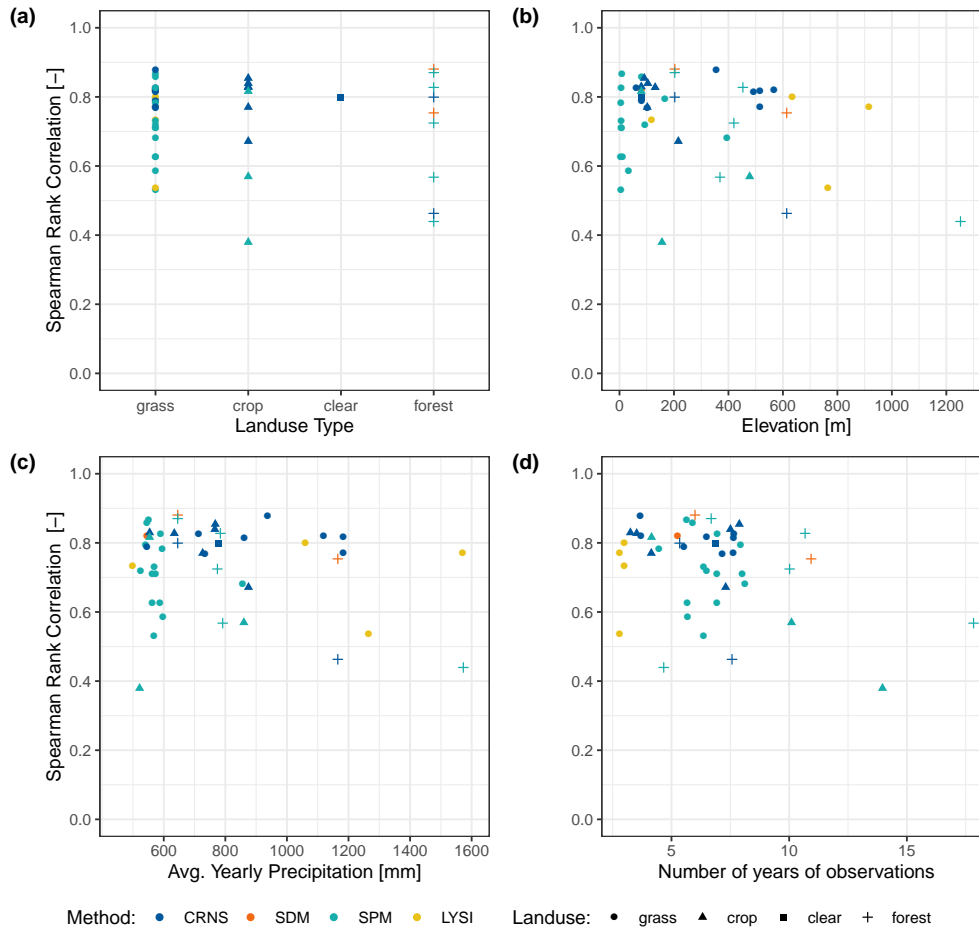


Figure 4. Spearman correlation coefficients of simulated versus observed de-seasonalized soilmoisture anomalies in dependence of its site characteristics: a) landuse, b) elevation and c) average yearly precipitation. See Table 3 for detailed overview per location. Colors denote the soil moisture data method (Cosmic Ray Neutron Sensing (CRNS), spatially distributed measurements (SDM), single profile measurements (SPM) and lysimeter (LYSI)) and shapes the landuse types reported at the locations (abbreviated as following: grass = grassland, clear= forest clearing, LYSI=Lysimeter).

Monthly Spearman correlation coefficients for all locations and measurement methods (n total=46) in 0–25 cm depth are presented in Fig. 5. The correlation coefficients show an apparent clear intra-annual variation, with the highest values in summer/autumn months, while the lowest values are found in winter months. The highest median correlation is detected in August (0.87), while the lowest correlations are found in January (0.37). The spread of the correlation coefficients within the different locations is largest in winter months, with some locations having very high correlations close to 1.0. Yet, in February and March, some locations show correlations below zero for the measurement methods CRNS, SPM and LYSI. The intra-annual variation of performance metrics was similar to the findings of Xia et al. (2014), that extensively evaluated simulated SM from four different hydrological models (Noah, Mosaic, SAC, VIC) in the North American Land Data Assimilation System

315 phase 2 (NLDAS-2) dataset, which is used for drought monitoring in the United States, with generally higher correlations in
 summer and lower correlations in winter. Lower correlations in winter can be related to higher uncertainties in simulations
 as well as observations with respect to frozen soils and snow cover. Annex Figure A3 shows correlations between simulated
 SM, CRNS and SDM. Low correlations between simulation and observations are accompanied by low correlations between
 the measurement methods, especially in winter. In a climate impact study investigating low flows over Europe, it could be
 320 shown that the overall uncertainty due to the selection of the hydrological model dominates the overall uncertainty including
 the meteorological drivers in snow dominated areas (Marx et al., 2018). Furthermore, the mHM model does not contain a full
 energy balance model, which limits the description of soil frost depths.

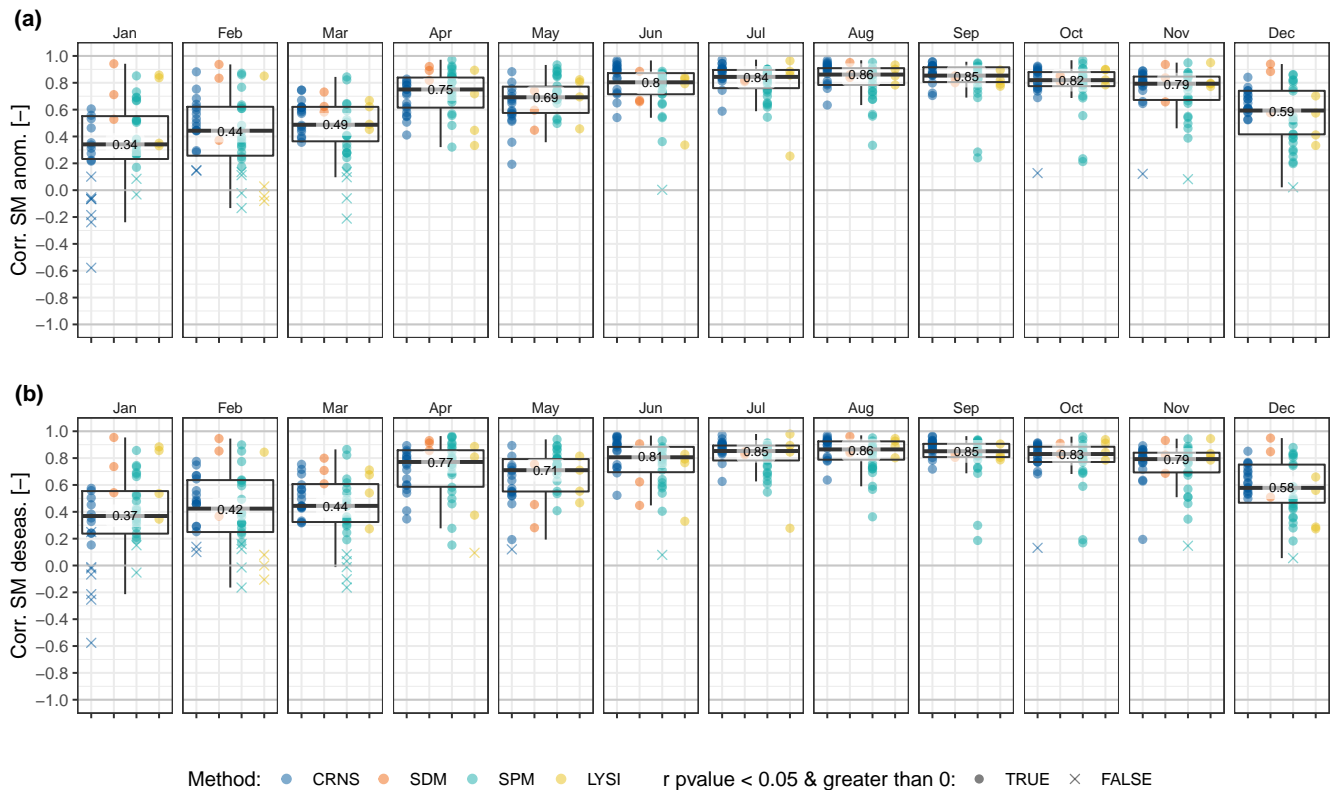


Figure 5. Comparison of the simulated mHM soil moisture ($0-25\text{cm}$) in the GDM-v2-2021 setup to observed SM anomalies without (a) and with (b) removing the mean seasonal SM cycle for each month depicted with boxplots. Values (x shapes) of each location colored by SM measurement method (CRNS: Cosmic Ray Neutron Sensing; SDM: spatially distributed measurements; SPM: single profile measurements; LYSI: Lysimeter) are shown. Sample sizes between measurement methods differ (CRNS: $n=16$, SDM: $n=3$, SPM: $n=23$; LYSI: $n=4$). Data points not fulfilling conditions of significant correlations ($p\text{-value} < 0.05$) and positive correlations are marked with x. See Figure A2 for additional plots separating the locations in subsets for detailed comparisons.

Observations using different SM measurement methods display considerable different correlations. The SPM generally scatter more, with large variation in winter and outliers with low performance in summer months. CRNS measurements show a consistently high performance in summer months but notably low correlations in winter (especially January). As snow days were removed from the time series in the CRNS measurements, the anomaly calculation from the remaining data was impacted by a smaller and incomplete sample size. Another reason for the observed lower correlations might be related to the variable penetration depth of CRNS ranging between 15 to 70 cm, depending on soil moisture (Köhli et al., 2015; Schrön et al., 2017). This could introduce systematic and temporally variable errors and deteriorate the correlation between observed and simulated soil water content (Baroni et al., 2018). The comparison to mHM top soil (0–25 cm) layer is still assumed a good compromise, since the soil water distribution is rather homogeneous between 0 and 25 cm under wet conditions, while under dry conditions the footprint is deeper and more heterogenous, but the highest sensitivity is still in the upper layers (exponential sensitivity). The SDM measurements show the most consistent performance across all months, except for May. This is illustrated in Figure A2 a), which displays only the locations Am Grossen Bruch and Hohes Holz, where both SDM and CRNS measurements are available. All measurement methods at these sites show in May and June a drop in correlations to the SM simulations while the observations have higher correlations between each other (see also A3). That points to deficiencies in the model, which may be related to the static vegetation module in mHM which does not include processes such as early onset of the growing season and related earlier depletion of the soil water storage. Figure A2 b) depicts the SPM data from FLUXNET and TERENO separately, which cover different time periods, 1997–2014 and 2011–2019, respectively. The performance at TERENO sites is generally higher compared to the FLUXNET sites. The intra-annual variation of the correlations is in good agreement among both monitoring networks and time periods. Higher correlations to SM simulations at the TERENO SPM sites may appear due to a larger number of sensors installed along the soil depth in the TERENO sites which may improve the vertical averaging of SM (see Table 3).

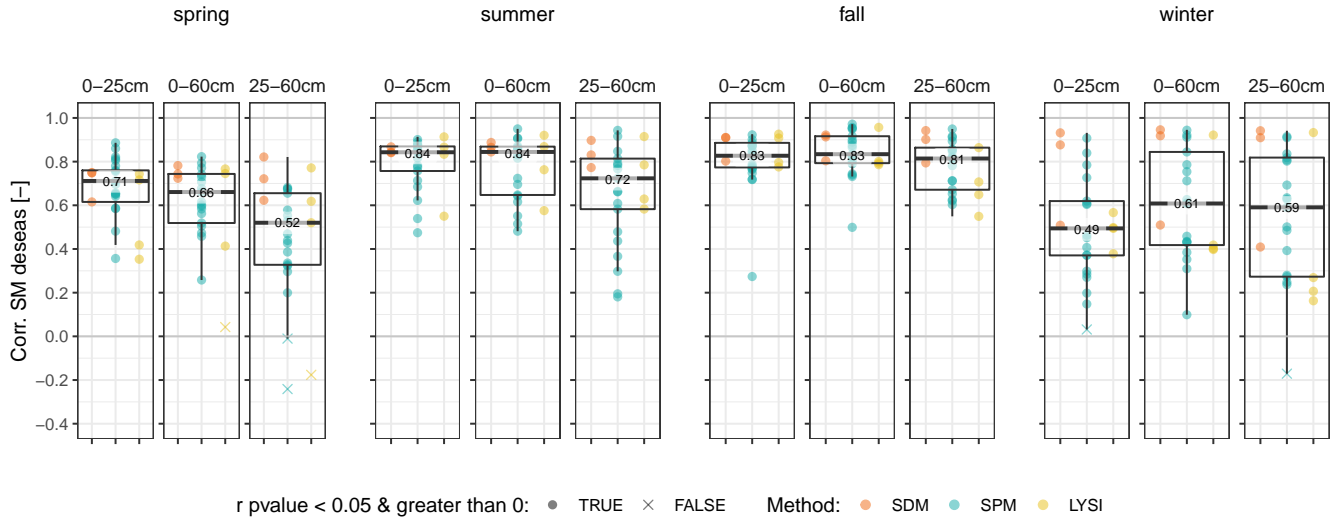


Figure 6. Spearman correlation coefficients of the simulated mHM soil moisture in the GDM-v2-2021 against observed deseasonalized soil moisture anomalies depicted with boxplots for three depths (0–25 cm, 0–60 cm, 25–60 cm). Values of each location are shown to enhance comparability between measurement methods as their sample sizes differ. Colours denote the source of soil moisture data (Methods: SDM: spatially distributed measurements; SPM: single profile measurements; LYSI: Lysimeter). Here only locations ($n=26$) are taken into account with measurements in 25–60 cm depth (SDM: $n=3$, SPM: $n=19$; LYSI: $n=4$). [Data points not fulfilling conditions of significant correlations \(\$p\text{-value} < 0.05\$ \) and positive correlations are marked with x.](#)

The Spearman correlation coefficients for each season and soil depth (0–25 cm, 25–60 cm and average over 0–60 cm) is depicted in Figure 6. Note, that here only locations were considered that have SM data in all depths and CRNS data was excluded as its varying penetration depth does not allow a consistent depth-wise evaluation, which leads to a smaller sample sizes of locations ($n=26$). Figure 6 shows that the median correlation is lower for the deeper soil moisture simulations when comparing the 0–25 cm to 25–60 cm depth for all seasons, except for winter during which the median R is higher in the lower 25–60 cm depth ($\Delta + 0.06$). In spring the lower depth 25–60 cm also shows strongest negative difference to the upper depth 0–25 cm in comparison to summer and autumn (Spring $\Delta - 0.19$, Summer $\Delta - 0.12$, Fall $\Delta - 0.02$). The correlations vary more in the 25–60 cm depth between locations in all seasons, with more outliers with very low correlations. Since the mHM was conceptualized for dominant processes at the large scale (mesoscale), not all processes that are important at the local scale are currently accounted for (e.g. variable rooting depths, lateral flow or groundwater soil water interaction). For instance, Rosenbaum et al. (2012) showed for the distributed SM measurements at the Wüstebach catchment that SM dynamics in the topsoil (5–50 cm depth) are influenced by groundwater. Processes of capillary rise are not modelled in mHM, hence it is expected that agreement to simulated SM by mHM at sites with groundwater-influence is lower compared to groundwater-distant sites. This effect should increase with depth due to increasing groundwater influence that could explain lower correlations in the 25–60 cm depth. Also, SPM sites might be affected more than SDM since these effects could be averaged out for SDM. Identification of groundwater characteristics at each measurement site was, however out of scope for this study. For the average across 0–60 cm

360 the correlations tend to be similar to 0–25 cm. Only in spring, correlations over the 0–60 cm soil column are lower compared to 0–25 cm due to the low correlations observed in 25–60 cm during this period. In Winter the average over 0–60 cm depth shows higher correlation than both 0–25 cm ($\Delta + 0.11$) and 25–60 cm ($\Delta + 0.02$) alone. The SDM overperform SPM and LYSI, with higher than average correlation values especially for the 25–60 cm depth, which underlines the assumption that local characteristics of single sensors e.g. groundwater influence and the resulting spatial variability of soil moisture (Famiglietti et al., 2008) are averaged out over a larger area and generally supports the closer scale match of SDM measurements and the 1.2×1.2 km² simulation grid cells. It has to be noted that the SPM at the same sites as the SDM also show comparable high correlation values (for an overview of the locations, see Table 3).

3.2 Comparison of different mHM model setups

In the following, the comparison between observations and the two model setups GDM-v1-2016 and GDM-v2-2021 (i.e., GDM version 1 and 2), as well as drought metrics between the two simulation setups are shown and discussed. Table 2 shows the median values of the Spearman correlation coefficients for different sub periods within the year (season, ~~vegetation-vegetative~~ active period April–October) and the full year. Considering all available SM data from all locations and measurement methods the median correlations between the two simulation setups slightly increase by +0.05 in GDM-v2-2021. The results on an intra-annual scale show a small decrease in the correlations in spring ($\Delta - 0.03$) and summer ($\Delta - 0.01$), but a significant increase of correlations in fall ($\Delta + 0.07$) and winter ($\Delta + 0.12$) in the new model setup. When analysing the metric over the ~~vegetation-and non-vegetation-vegetative and non-vegetative active~~ period (defined from April–October and November–March, respectively), the increase in median correlations is +0.03 and +0.10 (significant), respectively. Correlations using CRNS (n=16) and SPM (n=23) measurements support the overall findings. In general, the results show that the CRNS yield higher median correlation than the SPM measurements for both model setups, except for spring. While the median correlation in winter increased by +0.17 between GDM-v1-2016 to GDM-v2-2021 for CRNS, there is only a small increase in correlation of +0.03 for SPM. Similar results showing an overall increase in simulation performance were found by Albergel et al. (2012). In their study, the EMCWF operational and re-analysis SM product using the hydrological model H-TESSEL was improved due to changes in the soil hydrology in the model and an increase of model resolution. They concluded that a better representation of soil texture might obtain further improvements. Furthermore, De Lannoy et al. (2014) found moderate improvements in SM simulations compared to observations through implementing updated soil texture information.

Table 2. Median spearman correlation coefficients R of both simulated (GDM-v1-2016, GDM-v2-2021) versus observed deseasonalized soil moisture anomalies in depth 0–25 cm. Spearman correlation coefficients R are calculated annual, seasonal (spring=mam, summer=jja, fall=son, winter=djf) and the ~~vegetation~~-vegetative active period (defined from April–October and non-veg November–March). Note that some of the 40 locations have multiple soil moisture data sources (n = 46); see Table 3. Stars denote significant differences (p-value < 0.05) in correlations between the model setups according to paired Wilcoxon signed-rank test.

metric	method	setup	annual	spring	summer	fall	winter	non-veg	veg
R [-]	ALL (n=46)	GDM-v2-2021	0.78	0.65	0.85	0.84	0.49	0.59	0.84
		GDM-v1-2016	0.73	0.68	0.86	0.77	0.37	0.49	0.81
		Δ	+0.05	-0.03	-0.01	+0.07 (*)	+0.12 (*)	+0.10 (*)	+0.03
	CRNS (n=16)	GDM-v2-2021	0.81	0.63	0.88	0.86	0.60	0.65	0.86
		GDM-v1-2016	0.79	0.67	0.88	0.80	0.46	0.48	0.84
		Δ	+0.02	-0.04	0.0	+0.06 (*)	+0.14 (*)	+0.17 (*)	+0.02
	SPM (n=23)	GDM-v2-2021	0.72	0.67	0.79	0.78	0.39	0.45	0.82
		GDM-v1-2016	0.71	0.69	0.80	0.76	0.34	0.42	0.77
		Δ	+0.01	-0.02	-0.01	+0.02	+0.05	+0.03	+0.05

Next, we contrast the drought characteristics based on the two model setups to assess the differences in drought ranking and the spatial structure of drought events. Annual drought intensities aggregated over Germany based on the daily SMI using simulated SM from 1952 - 2020 are presented in Fig. 7 and grid-based for the last decade in Fig. 8 to compare the model setups in terms of drought classification. Fig. 7 shows only marginal differences between the model setups. They are slightly more prominent in the top soil compared to total soil column. The three years with the most intensive droughts largely agree. The ranking during the ~~vegetation~~-vegetative active period shows an exception due to the similar drought intensities in the years 1959, 1976 and 2003 in the top soil. The drought years are more pronounced with respect to drought intensities in the GDM-v2-2021 setup in the top soil, but in contrast, the average drought area is estimated larger in the GDM-v1-2016 setup in those years. Generally, the classification of drought years aggregated over Germany results in similar estimates using different operational drought monitor setups.

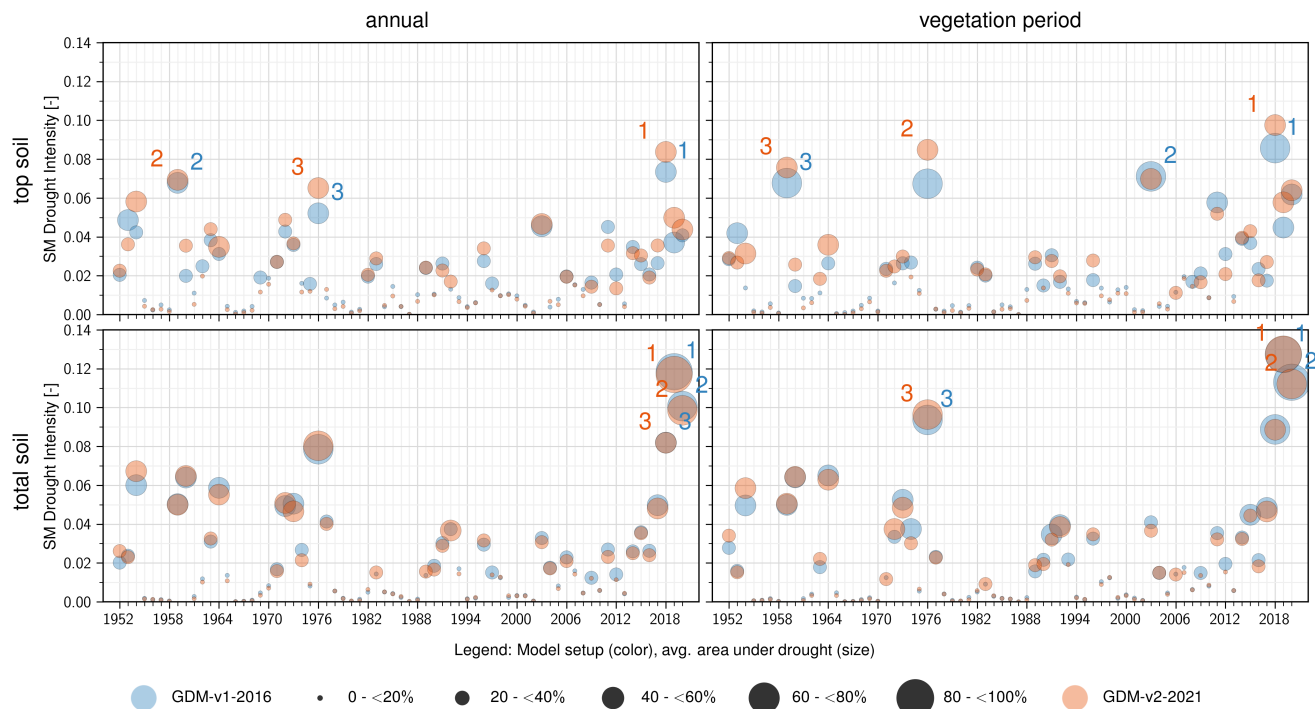


Figure 7. Soil moisture drought intensities spatially aggregated for Germany in the ~~vegetation~~-vegetative active period (April - October) in the top soil (5–25 cm) and total soil column (up to 2 m). The size of circles shows the average area under drought. The three largest drought events are denoted with numbers. Colours represent the two model setup GDM-v1-2016 and GDM-v2-2021. Colours are mixed when circles from both model setups overlay.

To assess regional differences in drought characteristics between the model setups, Fig. 8 shows the drought intensity maps in the ~~vegetation~~-vegetative active period for 2011–2020. Drought intensities are more spatially diverse in the GDM-v2-2021 setup that stem from the higher granularity of the GDM-v2-2021 setup with higher resolved soil information and less smoothed patterns than the GDM-v1-2016. Nevertheless, the general patterns are similar between the two setups, but regionally large differences can be seen (e.g., the drought intensities in the Swabian and Franconian Jura region are more pronounced concerning the neighbouring areas in the GDM-v1-2016 setup – see years 2017, 2019 total soil). Also, the differences in drought intensities are more pronounced in the total soil column in the last decade, which can be explained by multi-annual, cumulative effects. The current total soil drought lasts in many regions for at least three years. In Figure 9 the variance between grid cells for drought intensities during vegetation active period are shown as semi-variograms. In general, the spatial variance is larger in the total soil than top soil. The GDM-v2-2021 setup shows a general larger spatial variance between grid cells in the top soil and larger increase with distance (see Figure 9 (a)). The spatial variance in the total soil is lower at smaller distances in the GDM-v1-2016 setup, but slightly higher at larger distances. Figure 9 (b) showing semi-variance normalized by distance (and log scaled x-axis to to improve visibility of smaller distances) demonstrates that in the GDM-v2-2021 setup the

distance-normalized variance of drought intensities is increased especially at small spatial scale in both the top and total soil, indicating larger local differences in response to drought intensities. These findings are in line with Livneh et al. (2015) who investigated the influence of different soil databases on resulting hydrologic fluxes. They reported that the higher variability of soil properties in the finer soil database generally resulted in simulations with more considerable variability of (extreme) hydrologic responses.

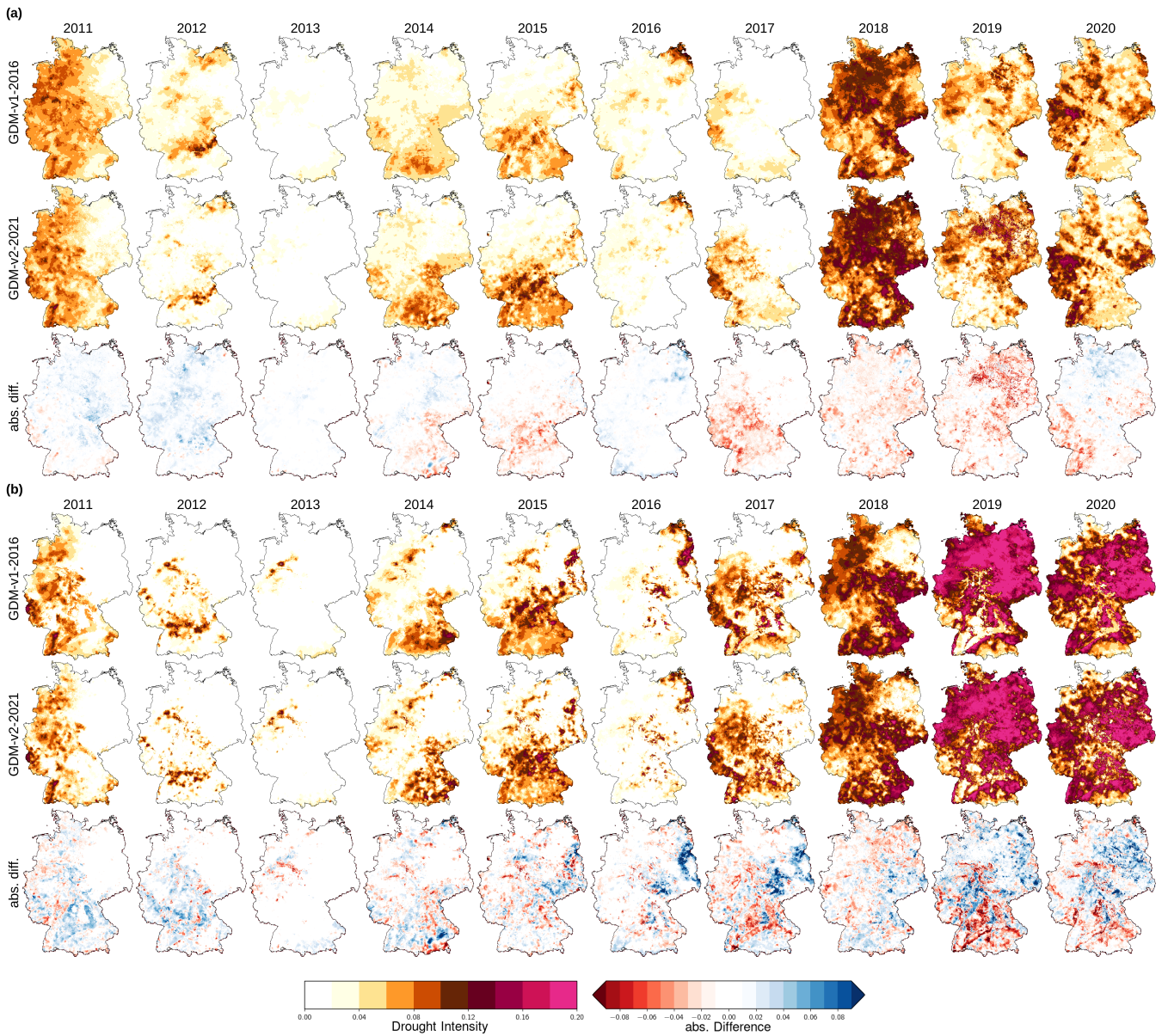


Figure 8. Soil moisture drought intensities (DI) per grid cell for (a) upper soil (5–25 cm) and (b) total soil column (up to 2 m) during ~~vegetation~~-vegetative active period (April -October) in the last decade (2011–2020) for the model setups GDM-v1-2016 and GDM-v2-2021 and absolute differences (GDM-v1-2016 - GDM-v2-2021). The GDM-v1-2016 data was remapped to the GDM-v2-2021 grid to calculate the differences. Graphs including all years from 1952 on can be found at <https://www.ufz.de/index.php?de=47252>

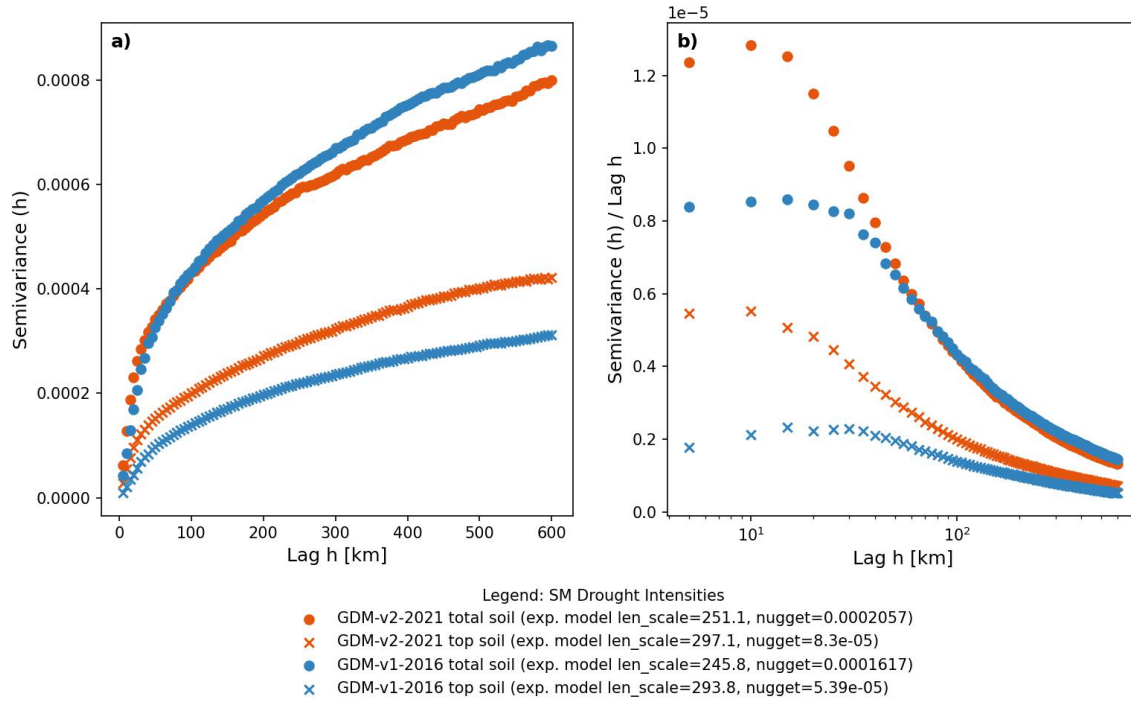


Figure 9. Empirical semi-variograms for drought intensities during vegetation active period in upper Soil for GDM-v1-2016 and GDM-v2-2021 setup. The bin size was set to 5 km (nearest larger even km bin size relative to the GDM-v2-2016 modelling resolution). The length scale and nugget of the fitted exponential theoretical semi-variograms are noted in the legend. In Subplot b) the y and x axis are log scaled.

Table 3. Overview of soil moisture measurement sites. Method denotes the different data sources: Cosmic Ray Neutron Sensing (CRNS), spatially distributed measurements (SDM), single profile measurements (SPM) and lysimeter (LYSI) (see method section for detailed description). The group denotes the experimental site network (for TERENO: GC = Central Germany; Rur/E = Rur/Eifel; NE = Northeast, PAO = Pre Alpine Observatory) and land use shows site characteristics (grass = grassland, crop = cropland, DBF = Deciduous Broadleaved Forest, ENF = Evergreen Needled Forest, clear = clearing). For Fluxnet, the original site name is denoted in brackets. Sensor depths and numbers are denoted. R Spearman correlation coefficients of comparing simulated versus observed de-seasonalized soil moisture anomalies in the GDM-v2-2021 setup shown are based on the whole period for 0–25 cm and 25–60 cm depth.

network	site	method	land use	begin	end	availability	data n	elevation	precipitation	sensor n	sensor depth		R	
											0–25 cm	25–60 cm	0–25 cm	25–60 cm
TERENO GC	BadLauchstädt	LYSI	crop	2016-01-01	2018-12-31	100 %	1091	118 m	498 mm	3	10	30, 50	0.73	0.71
	Ermsleben	SPM	grass	2012-01-25	2019-12-31	81 %	2343	167 m	541 mm	1	10, 20	30, 40, 50, 60	0.80	0.68
	Am Grossen Bruch	CRNS	grass	2014-06-24	2019-11-28	95 %	1892	81 m	545 mm				0.79	-
		SDM		2014-07-30	2019-11-18	84 %	1618			20	var.	var.	0.82	0.84
		SPM		2014-02-07	2019-12-31	98 %	2114			1	10, 20	30, 40, 50	0.86	0.85
	Hecklingen	SPM	grass	2013-07-05	2019-12-31	94 %	2223	93 m	525 mm	1	10, 20	30, 40, 50	0.72	0.71
	HohesHolz	CRNS	DBF	2014-08-27	2019-11-28	91 %	1745	203 m	645 mm				0.80	-
		SDM		2012-07-20	2019-12-30	96 %	2613			39	var.	var.	0.88	0.86
		SPM		2013-04-25	2019-12-31	97 %	2358			2	10, 20	30, 40, 50	0.87	0.88
	Hordorf	CRNS	crop	2016-09-29	2019-11-28	88 %	1022	80 m	554 mm				0.83	-
		SPM		2015-11-06	2019-12-31	98 %	1493			1	10, 20	30, 40, 50	0.82	0.74
TERENO Rur/E	Aachen	CRNS	crop	2012-01-13	2019-05-01	91 %	2437	216 m	875 mm				0.67	-
	Gevenich	CRNS	crop	2011-07-06	2019-01-04	91 %	2496	104 m	766 mm				0.84	-
	Heinsberg	CRNS	grass	2011-09-08	2019-05-01	94 %	2628	61 m	712 mm				0.83	-
	Kall	CRNS	grass	2011-09-14	2019-05-01	78 %	2185	492 m	861 mm				0.82	-
	Kleinau	CRNS	grass	2015-08-25	2019-04-26	87 %	1169	355 m	937 mm				0.88	-
	Merzenhausen	CRNS	crop	2011-05-18	2019-04-03	90 %	2597	91 m	767 mm				0.85	-
	Rollesbr1	CRNS	grass	2011-05-18	2018-12-31	87 %	2409	516 m	1183 mm				0.77	-
	Rollesbr2	CRNS	grass	2012-06-30	2018-12-25	86 %	2045	516 m	1183 mm				0.82	-
	Ruraue	CRNS	grass	2011-11-08	2019-01-01	90 %	2340	102 m	734 mm				0.77	-
	Schoeneseiffen	CRNS	grass	2015-08-13	2019-04-25	83 %	1120	567 m	1119 mm				0.82	-
	Selhausen	CRNS	crop	2015-03-06	2019-04-26	95 %	1441	102 m	726 mm				0.77	-
	Wildenrath	CRNS	clear	2012-05-11	2019-03-23	91 %	2273	79 m	776 mm				0.80	-
	Wüstenbach	CRNS	ENF	2011-03-12	2018-10-05	79 %	2173	614 m	1165 mm				0.44	-
		SDM		2009-01-27	2019-12-31	100 %	3989			150	10, 20 (2x)	50	0.75	0.74
TERENO NE	AltTellin	SPM	grass	2014-05-10	2019-12-30	90 %	1859	9 m	551 mm	1	10, 20	30, 40, 50	0.87	0.26
	Bentzin	SPM	grass	2013-08-19	2019-12-30	98 %	2281	5 m	568 mm	1	10, 20	30, 40, 50, 60	0.53	0.77
	Droennewitz	SPM	grass	2014-04-12	2019-12-30	73 %	1519	33 m	598 mm	1	10, 20	30, 40, 50, 60	0.59	0.66
	Goermin	SPM	grass	2013-08-19	2019-12-30	95 %	2207	7 m	569 mm	1	10, 20	30, 40, 50, 60	0.73	0.47
	Leppin	SPM	grass	2013-01-28	2019-12-30	96 %	2420	6 m	563 mm	1	10, 20	30, 40, 50, 60	0.71	0.53
	Medrow	SPM	grass	2015-07-13	2019-12-30	100 %	1627	5 m	595 mm	1	10, 20	30, 40, 50, 60	0.78	0.76
	Muehlenkamp	SPM	grass	2012-01-01	2019-12-30	82 %	2388	8 m	574 mm	1	10, 20	30, 40, 50, 60	0.71	0.37
	Ueckeritz	SPM	grass	2013-01-28	2019-12-30	93 %	2349	4 m	562 mm	1	10, 20	30, 40, 50, 60	0.63	0.61
	Wotenick	SPM	grass	2014-04-30	2019-12-30	95 %	1964	11 m	588 mm	1	10, 20	30, 40, 50, 60	0.63	0.51
	Zarnckla	SPM	grass	2013-01-23	2019-12-30	95 %	2404	6 m	590 mm	1	10, 20	30, 40, 50, 60	0.83	0.77
TERENO PAO	Fendt	LYSI	grass	2017-01-01	2019-12-31	100 %	1090	634 m	1059 mm	18	10	30, 50	0.80	0.7
	Graswang	LYSI	grass	2017-03-17	2019-12-31	93 %	948	916 m	1570 mm	6	10	30, 50	0.77	0.66
	Rottenbuch	LYSI	grass	2017-03-17	2019-12-31	93 %	948	765 m	1265 mm	12	10	30, 50	0.54	0.53
FLUXNET	Gebesee (DE-Geb)	SPM	crop	2001-01-16	2014-12-31	91 %	4657	156 m	522 mm	1	8, 16	32	0.38	0.33
	Grillenburg (DE-Gri)	SPM	grass	2006-11-21	2014-12-31	98 %	2891	394 m	856 mm	1	10	-	0.68	-
	Hainich (DE-Hai)	SPM	DBF	2002-12-27	2012-12-31	98 %	3570	420 m	774 mm	1	8, 16	32	0.72	0.57
	Klingenberg (DE-Kli)	SPM	crop	2004-11-27	2014-12-31	87 %	3208	478 m	860 mm	1	10	-	0.57	-
	Lackenberg (DE-Lkb)	SPM	ENF	2009-05-01	2013-12-31	90 %	1533	1252 m	1573 mm	1	4	-	0.44	-
	Leinefelde (DE-Lnf)	SPM	DBF	2002-05-01	2012-12-31	72 %	2796	453 m	784 mm	1	8, 16	32	0.83	0.77
	Tharandt (DE-Tha)	SPM	ENF	1997-03-06	2014-12-31	95 %	6189	369 m	791 mm	1	10	-	0.57	-
DWD	Cunnersdorf	CRNS	crop	2016-06-23	2019-12-31	95 %	1217	131 m	634 mm				0.83	0.68

4 Summary and Conclusions

415 This study ~~presents an evaluation of~~ evaluates soil moisture (SM) dynamics from two mHM model simulations from operational GDM setups. The comparisons between observed and simulated SM are conducted using various ground-based SM observations (n total = 46) with multiple measurement methods and different climate gradients. The simulated and observed SM dynamics agreement is especially high in the ~~vegetation~~ vegetative active period (median R 0.84 in GDM-v2-2021) and lower in winter (median R 0.59 in GDM-v2-2021). The improvements in capturing observed SM dynamics between the model
420 setups GDM-v1-2016 to GDM-v2-2021 showed that an increased input soil data resolution (BUEK1000 to BUEK200) in combination with increased modelling resolution ($4 \times 4 \text{ km}^2$ to $\approx 1.2 \times 1.2 \text{ km}^2$) not only produces simulated SM in similar quality as the lower resolution model setup but enhances the model accuracy to simulate SM dynamics. We identified significant improvements between the first and second GDM versions to observed SM, with enhanced correlations during fall (+0.07 median) and winter (+0.12 median). However, the overall improvements were relatively small, partly because the lower res-
425 olution model setup ($4 \times 4 \text{ km}$ grid cells) was already capturing the observed SM dynamics well. Annual drought statistics and ranking based on drought intensities and average area under drought computed on the time frame ~~1952–2020 was~~ 1952–2020 were robust between the model setups, with only minor differences on the scale of Germany. The spatial structures in the higher resolved GDM-v2-2021 setup, including an updated soil map, display larger granularity and spatially more diverse responses to drought, allowing a more refined representation of spatial SM heterogeneity. The higher spatial resolution that is achieved is
430 of great relevance, especially concerning local risk assessments.

We focused the model comparisons on analyzing SM dynamics for their relevance for SM droughts, which are defined as a negative deviation from normal SM conditions. A way forward to better absolute estimations of simulated SM (that was not investigated here), which could improve the model internal flux partitioning, can be the integration of observed SM data in the model calibration itself, ~~which has been demonstrated.~~ This kind of approach has been successfully demonstrated using, e.g.
435 CRNS data in the Rur catchment in Germany (Baatz et al., 2017) or remotely sensed SM in the Danube catchment (Wanders et al., 2014). An extended model validation of the SM component of mHM forced with onsite precipitation, local soil maps with soil physical property information on even higher resolution (e.g. BUEK25 or BUEK50) would help to further understand current limitations of mHM to model SM dynamics and separate the analyses from the limited data availability at the scale of Germany.

440 The results prominently underline the importance of long-term measurement series for developing and optimising such data products as the GDM. Good coverage of relevant environmental gradients with suitable measurement networks is essential, especially because of rapidly changing environmental conditions. The direct comparison of the different measurement methods for recording soil moisture showed the importance of measurement methods such as CRNS or SDM, which allow better estimates of mean soil moisture conditions to be determined for larger areas. Also, the temporal availability concerning record
445 lengths and spatial availability, e.g. national coverage of spatially representative SDM and CRNS measurements still limits the studies, such as the one presented here, in terms of statistical robustness. Furthermore, we did not analyze deeper soil depths ($> 60 \text{ cm}$), because most measurement sites do not have SM data in these depths. Continuous improvements of the SM

observational database will be beneficial for future hydrological model evaluations. For future studies, a solution to the variable penetration depth of CRNS could be to compare observed and simulated neutron counts directly by using the COSMIC forward model (Shuttleworth et al., 2013). It is designed to account for irregular soil moisture profiles in all modelled depth layers. While COSMIC has been already implemented in mHM, its proper parameterization would require dedicated research and is out of the scope of this study, where we focus on first-order comparisons to conventional soil moisture products. Regarding the SDM measurements, a source of uncertainty lies in ~~the calculation of~~ calculating the spatially averaged value. The mean calculation is critical due to ~~an unstable a varying~~ number of available sensors in the measurement grids over time. A robust mean calculation with advanced sensor weighting is currently the subject of research.

~~To~~ Several questions arise to further improve SM states' simulations with mHM on a national scale in Germany (or larger ~~);~~ ~~several questions arise~~ towards a continental scale). What are the limitations ~~for of~~ the operational German-wide model setup concerning model input data? What are the current limitations of process representation? Which hydrological processes become relevant at smaller scales? A decisive input that influences hydrological model performance is precipitation (Mo et al., 2012). Model performance of mHM was related to rain gauge density on a European scale by Rakovec et al. (2016). While Germany has a very dense meteorological station network, local precipitation can still differ significantly from the interpolated products. Even though, Samaniego et al. (2013) showed that the interpolation results on daily precipitation data here compared to the high resolution German Weather Service reanalysis product REGNIE (Rauthe et al., 2013) only differ marginally, the difference of local precipitation from interpolated values is expected to have a large influence on SM dynamics. Thus, improvements in the interpolated precipitation may result in increased model performance. Besides ~~that~~, we may achieve a more precise estimation of potential evapotranspiration ~~through~~ by implementing the Penman-Monteith methods.

Finally, we ~~constitute~~ conclude that the resolution of $\approx 1.2 \times 1.2 \text{ km}^2$ is currently the best compromise between the need for increased model resolution (user perspective) and the current data ~~availability~~ availability and process representation in mHM (scientific perspective). We emphasise the need for continuous dialogues between stakeholders and the scientific community to improve the underlying model system as well as the provision of user-tailored drought information.

Appendix A: Appendix

A1

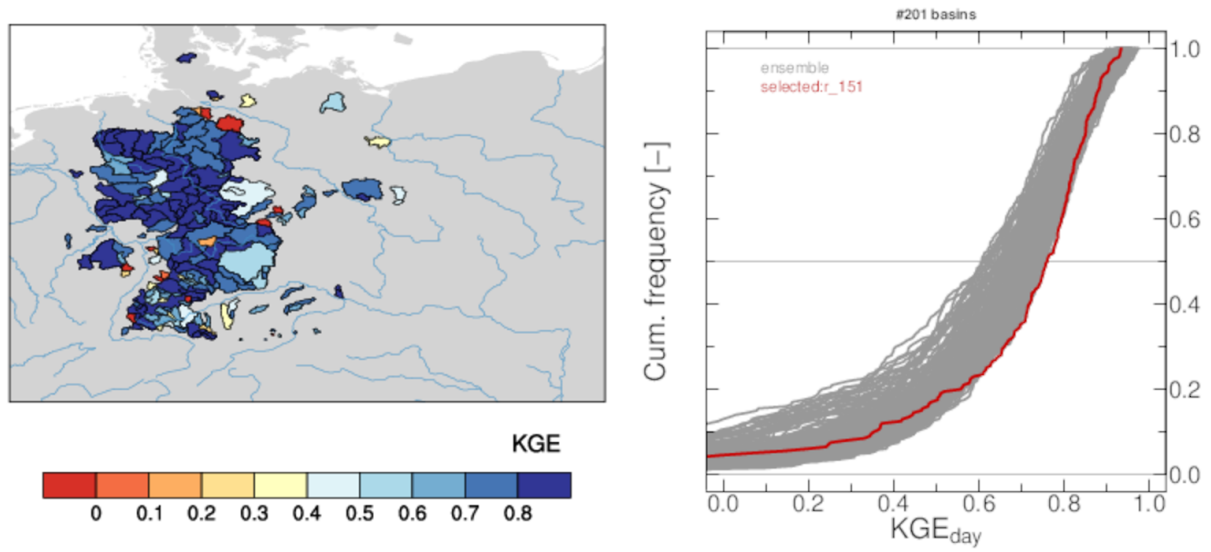


Figure A1. Results of mHM multibasin model calibration based on streamflow data from 201 catchments. Left: spatial map of KGE for each basin. Right: KGE Cumulative density function of setup 200 parameter sets, generated by random sampling of the basins. Bold red marks the selected parameter set.

475 Spearman correlation coefficients of simulated versus observed deseasonalized soilmoisture anomalies in dependence of its site characteristics: landuse, elevation and yearly precipitation. See table 3 in the Appendix for detailed overview per location. Colors denote the soil moisture data method (Cosmic Ray Neutron Sensing (CRNS), spatially distributed measurements (SDM), single profile measurements (SPM) and lysimeter (LYSI)) and shapes the landuse types (abbreviated as following: grass = grassland, clear = forest clearing, LYSI=Lysimeter).

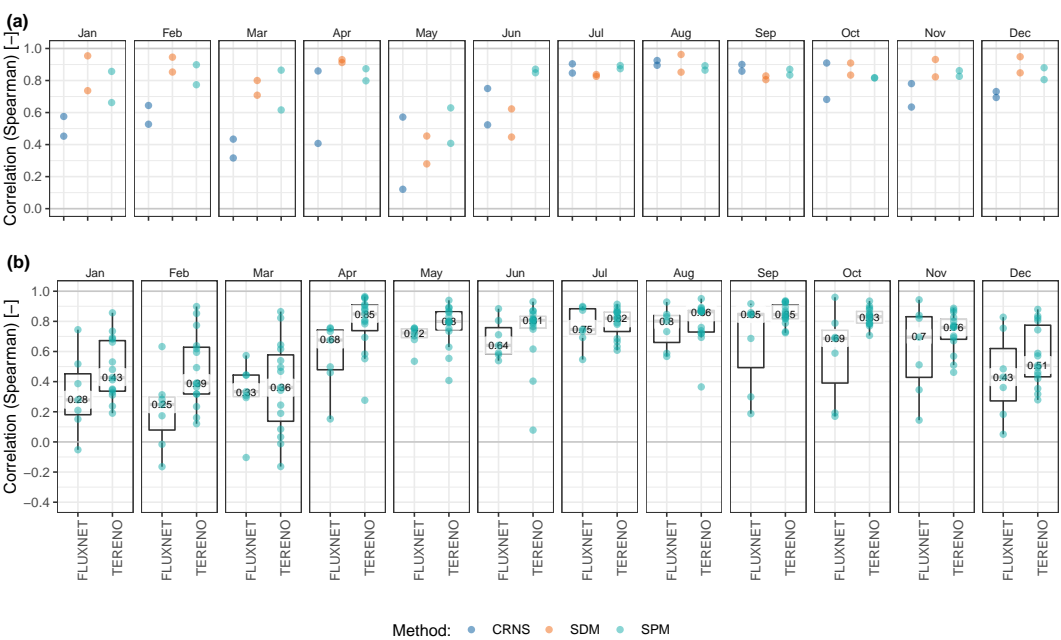


Figure A2. Spearman correlation coefficients of simulated soil moisture by mHM in the GDM-v2-2021 setup versus observed deseasonalized soil moisture anomalies for each month as a supplement to fig. 5 by a) comparing locations Hohes Holz and Am Grossen Bruch equipped with CRNS, spatially distributed and single profile measurements of soil moisture and b) comparing FLUXNET (n=7) and TERENO (n=20) SPM data.

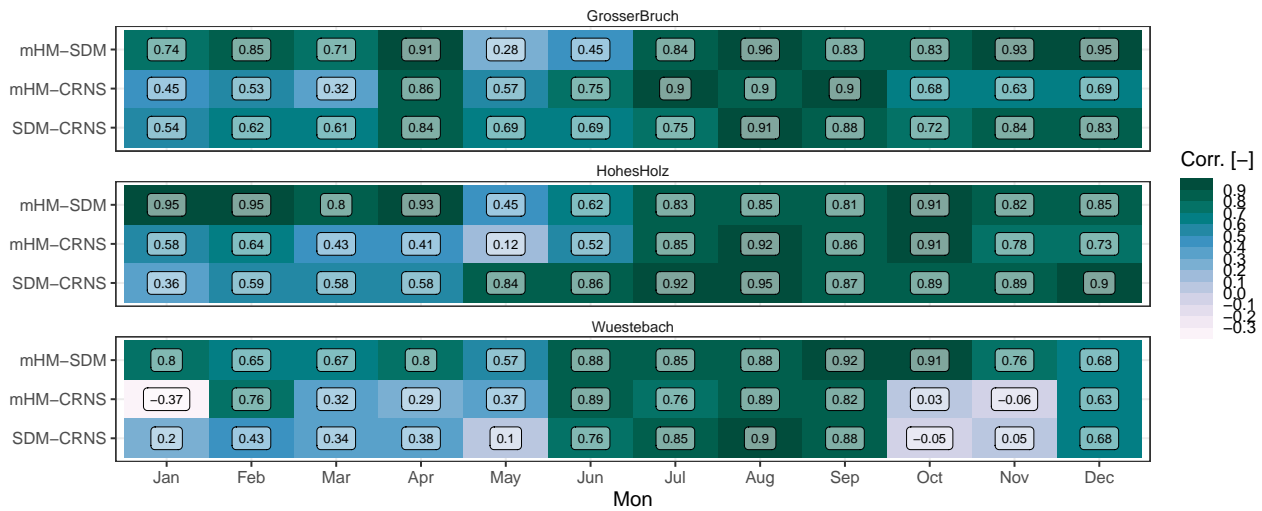


Figure A3. Monthly spearman correlation coefficients for years 2014 - 2019 on deseasonalized SM anomalies simulated by mHM against SM observations from CRNS and SDM measurements and between the SM observations for the three locations Am Grossen Bruch, Hohes Holz and Wüstebach that have both CRNS and SDM measurements available.

Code and data availability. Observational and simulated SM data (<https://www.doi.org/10.48758/ufz.12541>) as well as simulated SMI drought characteristics (DOI: <https://www.doi.org/10.48758/ufz.12534>) that were used in the study are available in UFZ Data Investigation Portal.

480 Open-source mHM code is available at <https://github.com/mhm-ufz> and SMI code <https://doi.org/10.5281/zenodo.5842486>. TERENO and FLUXNET soil moisture data can be obtained at <https://ddp.tereno.net/ddp/> and <https://fluxnet.org/>, respectively.

Author contributions. F.B., L.S., A.H., C.R., M.S., A.M., R.Kumar developed the concept for the manuscript; F.B. conducted simulations, SM data compilation, data analyses, first manuscript drafts; O.R., F.B. L.S., R.Kumar, A.M. contributed to develop the GDM-v2-2021 setup; O.R. calibrated the GDM-v2-2021 setup; R.Kumar., M.S., O.R., A.M., A.H., L.S., S.T. helped to improve the analyses and manuscript; S.M.

485 and S.T. supported mHM model development and technical maintenance of the GDM; M.S., C.R., R.Kiese, K.S., H.B. provided SM observation data and helped with interpreting the data/improve the manuscript; S.Z. assisted answering questions related to soil processes and improve the manuscript.

Competing interests. The authors declare that they have no conflict of interest.

Acknowledgements. This work is partly funded by Helmholtz-Climate-Initiative (HI-CAM) in the Helmholtz Associations Initiative and

490 Networking Fund. The authors are responsible for the content of this publication. We acknowledge the TERENO community and FLUXNET community for providing soil moisture observational data. Special ~~acknowledgment~~[acknowledgment](#) goes to Hans-Jörg Vogel (UFZ), René Zahl (UFZ), Christian Hohmann (GFZ), Ingo Heinrich (GFZ) and Falk Böttcher (DWD) for providing soil moisture observations. We kindly acknowledge the German Weather Service (DWD), the European Environmental Agency (EEA), the Federal Institute for Geosciences and Natural Resources (BGR), the Federal Agency for Cartography and Geodesy (BKG), the European Space Agency (ESA), the U.S.

495 Geological Survey (USGS), the Global Runoff Data Centre (GRDC) as data providers. [The scientific results have \(in part\) been computed at the High-Performance Computing \(HPC\) Cluster EVE, a joint effort of both the Helmholtz Centre for Environmental Research - UFZ \(<http://www.ufz.de/>\) and the German Centre for Integrative Biodiversity Research \(iDiv\) Halle-Jena-Leipzig \(<http://www.idiv-biodiversity.de/>\). We would like to thank the administration and support staff of EVE who keep the system running and support us with our scientific computing needs: Thomas Schnicke, Ben Langenberg, Guido Schramm, Toni Harzendorf, Tom Stempel and Lisa Schurack from the UFZ, and Christian Krause from iDiv. Finally, we want to thank two anonymous reviewers and the Editor for their constructive comments, which improved the quality of this study.](#)

500

References

- Albergel, C., De Rosnay, P., Balsamo, G., Isaksen, L., and Muñoz-Sabater, J.: Soil moisture analyses at ECMWF: Evaluation using global ground-based in situ observations, *Journal of Hydrometeorology*, 13, 1442–1460, <https://doi.org/10.1175/JHM-D-11-0107.1>, 2012.
- 505 Andreasen, M., Jensen, K. H., Desilets, D., Franz, T. E., Zreda, M., Bogen, H. R., and Looms, M. C.: Status and Perspectives on the Cosmic-Ray Neutron Method for Soil Moisture Estimation and Other Environmental Science Applications, *Vadose Zone Journal*, 16, vzj2017.04.0086, <https://doi.org/https://doi.org/10.2136/vzj2017.04.0086>, <https://acsess.onlinelibrary.wiley.com/doi/abs/10.2136/vzj2017.04.0086>, 2017.
- Baatz, R., Bogen, H. R., Hendricks Franssen, H., Huisman, J. A., Montzka, C., and Vereecken, H.: An empirical vegetation correction for soil water content quantification using cosmic ray probes, *Water Resources Research*, 51, 2030–2046, <https://doi.org/10.1002/2014WR016443>, <https://onlinelibrary.wiley.com/doi/abs/10.1002/2014WR016443>, 2015.
- 510 Baatz, R., Hendricks Franssen, H.-J., Han, X., Hoar, T., Bogen, H. R., and Vereecken, H.: Evaluation of a cosmic-ray neutron sensor network for improved land surface model prediction, *Hydrology and Earth System Sciences*, 21, 2509–2530, <https://doi.org/https://doi.org/10.5194/hess-21-2509-2017>, <https://hess.copernicus.org/articles/21/2509/2017/>, 2017.
- 515 Baldocchi, D., Falge, E., Gu, L., Olson, R., Hollinger, D., Running, S., Anthoni, P., Bernhofer, C., Davis, K., Evans, R., Fuentes, J., Goldstein, A., Katul, G., Law, B., Lee, X., Malhi, Y., Meyers, T., Munger, W., Oechel, W., U. K. T. P., Pilegaard, K., Schmid, H. P., Valentini, R., Verma, S., Vesala, T., Wilson, K., and Wofsy, S.: FLUXNET: A New Tool to Study the Temporal and Spatial Variability of Ecosystem-Scale Carbon Dioxide, Water Vapor, and Energy Flux Densities, *Bulletin of the American Meteorological Society*, 82, 2415–2434, [https://doi.org/10.1175/1520-0477\(2001\)082<2415:FANTTS>2.3.CO;2](https://doi.org/10.1175/1520-0477(2001)082<2415:FANTTS>2.3.CO;2), https://journals.ametsoc.org/view/journals/bams/82/11/1520-0477_2001_082_2415_fantts_2_3_co_2.xml, 2001.
- 520 Baroni, G., Scheffele, L., Schrön, M., Ingwersen, J., and Oswald, S.: Uncertainty, sensitivity and improvements in soil moisture estimation with cosmic-ray neutron sensing, *Journal of Hydrology*, 564, 873–887, <https://doi.org/10.1016/j.jhydrol.2018.07.053>, <https://linkinghub.elsevier.com/retrieve/pii/S0022169418305675>, 2018.
- BGR: Digital soil map of Germany 1 : 1,000,000 (BUEK 1000), 1998.
- 525 BGR: Hydrogeological map of Germany: 200,000 (HUEK 200), 2009.
- BGR: Digital soil map of Germany 1 : 200,000 (BUEK 200) v0.5, 2020.
- BKG: Digital Elevation Model (DEM), 2010.
- Boergens, E., Güntner, A., Dobslaw, H., and Dahle, C.: Quantifying the Central European Droughts in 2018 and 2019 With GRACE Follow-On, *Geophysical Research Letters*, 47, <https://doi.org/10.1029/2020GL087285>, 2020.
- 530 Bogen, H., Herbst, M., Huisman, J., Rosenbaum, U., Weuthen, A., and Vereecken, H.: Potential of Wireless Sensor Networks for Measuring Soil Water Content Variability, *Vadose Zone Journal*, 9, 1002–1013, <https://doi.org/10.2136/vzj2009.0173>, <http://doi.wiley.com/10.2136/vzj2009.0173>, 2010.
- Bogen, H., Montzka, C., Huisman, J., Graf, A., Schmidt, M., Stockinger, M., von Hebel, C., Hendricks-Franssen, H., van der Kruk, J., Tappe, W., Lücke, A., Baatz, R., Bol, R., Groh, J., Pütz, T., Jakobi, J., Kunkel, R., Sorg, J., and Vereecken, H.: The TERENO-Rur Hydrological Observatory: A Multiscale Multi-Compartment Research Platform for the Advancement of Hydrological Science, *Vadose Zone Journal*, 17, 180055, <https://doi.org/10.2136/vzj2018.03.0055>, <http://doi.wiley.com/10.2136/vzj2018.03.0055>, 2018.
- 535 Bogen, H. R.: TERENO: German network of terrestrial environmental observatories, *Journal of large-scale research facilities JLSRF*, 2, 52, <https://doi.org/10.17815/jlsrf-2-98>, <http://jlsrf.org/index.php/lrf/article/view/98>, 2016.

- Bogena, H. R., Huisman, J. A., Baatz, R., Hendricks Franssen, H.-J., and Vereecken, H.: Accuracy of the cosmic-ray soil water content probe in humid forest ecosystems: The worst case scenario: Cosmic-Ray Probe in Humid Forested Ecosystems, *Water Resources Research*, 49, 5778–5791, <https://doi.org/10.1002/wrcr.20463>, <http://doi.wiley.com/10.1002/wrcr.20463>, 2013.
- Bogena, H. R., Huisman, J. A., Güntner, A., Hübner, C., Kusche, J., Jonard, F., Vey, S., and Vereecken, H.: Emerging methods for noninvasive sensing of soil moisture dynamics from field to catchment scale: a review, *WIREs Water*, 2, 635–647, <https://doi.org/10.1002/wat2.1097>, <https://onlinelibrary.wiley.com/doi/10.1002/wat2.1097>, 2015.
- Bogena, H. R., Schrön, M., Jakobi, J., Ney, P., Zacharias, S., Andreasen, M., Baatz, R., Boorman, D., Duygu, M. B., Eguibar-Galán, M. A., Fersch, B., Franke, T., Geris, J., González Sanchis, M., Kerr, Y., Korf, T., Mengistu, Z., Mialon, A., Nasta, P., Nitychoruk, J., Pisinaras, V., Rasche, D., Rosolem, R., Said, H., Schattan, P., Zreda, M., Achleitner, S., Albentosa-Hernández, E., Akyürek, Z., Blume, T., del Campo, A., Canone, D., Dimitrova-Petrova, K., Evans, J. G., Ferraris, S., Frances, F., Gisolo, D., Güntner, A., Herrmann, F., Iwema, J., Jensen, K. H., Kunstmann, H., Lidón, A., Looms, M. C., Oswald, S., Panagopoulos, A., Patil, A., Power, D., Rebmann, C., Romano, N., Scheffele, L., Seneviratne, S., Weltin, G., and Vereecken, H.: COSMOS-Europe: a European network of cosmic-ray neutron soil moisture sensors, *Earth System Science Data*, 14, 1125–1151, <https://doi.org/10.5194/essd-14-1125-2022>, <https://essd.copernicus.org/articles/14/1125/2022/>, 2022.
- Cammalleri, C., Micale, F., and Vogt, J.: On the value of combining different modelled soil moisture products for European drought monitoring, *Journal of Hydrology*, 525, 547–558, <https://doi.org/10.1016/j.jhydrol.2015.04.021>, <http://dx.doi.org/10.1016/j.jhydrol.2015.04.021>, publisher: Elsevier B.V., 2015.
- De Lannoy, G. J. M., Koster, R. D., Reichle, R. H., Mahanama, S. P. P., and Liu, Q.: An updated treatment of soil texture and associated hydraulic properties in a global land modeling system, *Journal of Advances in Modeling Earth Systems*, 6, 957–979, <https://doi.org/10.1002/2014MS000330>, <http://doi.wiley.com/10.1002/2014MS000330>, 2014.
- Dembélé, M., Ceperley, N., Zwart, S. J., Salvatore, E., Mariethoz, G., and Schaeffli, B.: Potential of satellite and reanalysis evaporation datasets for hydrological modelling under various model calibration strategies, *Advances in Water Resources*, 143, 103 667, <https://doi.org/10.1016/j.advwatres.2020.103667>, <https://linkinghub.elsevier.com/retrieve/pii/S030917082030230X>, 2020.
- Desilets, D., Zreda, M., and Ferré, T. P. A.: Nature’s neutron probe: Land surface hydrology at an elusive scale with cosmic rays: NATURE’S NEUTRON PROBE, *Water Resources Research*, 46, <https://doi.org/10.1029/2009WR008726>, <http://doi.wiley.com/10.1029/2009WR008726>, 2010.
- Dimitrova-Petrova, K., Geris, J., Wilkinson, M. E., Rosolem, R., Verrot, L., Lilly, A., and Soulsby, C.: Opportunities and challenges in using catchment-scale storage estimates from cosmic ray neutron sensors for rainfall-runoff modelling, *Journal of Hydrology*, 586, 124 878, <https://doi.org/10.1016/j.jhydrol.2020.124878>, <https://linkinghub.elsevier.com/retrieve/pii/S0022169420303383>, 2020.
- EEA: CORINE Land Cover 1990, 2000 and 2006, 2009.
- ESA: Global Land Cover Map for 2009, http://due.esrin.esa.int/files/Globcover2009_V2.3_Global_.zip, 2009.
- Famiglietti, J. S., Ryu, D., Berg, A. A., Rodell, M., and Jackson, T. J.: Field observations of soil moisture variability across scales: SOIL MOISTURE VARIABILITY ACROSS SCALES, *Water Resources Research*, 44, <https://doi.org/10.1029/2006WR005804>, <https://onlinelibrary.wiley.com/doi/10.1029/2006WR005804>, 2008.
- Grillakis, M. G.: Increase in severe and extreme soil moisture droughts for Europe under climate change, *Science of The Total Environment*, 660, 1245–1255, <https://doi.org/10.1016/j.scitotenv.2019.01.001>, <https://linkinghub.elsevier.com/retrieve/pii/S0048969719300014>, 2019.

- 575 Gupta, H. V., Kling, H., Yilmaz, K. K., and Martinez, G. F.: Decomposition of the mean squared error and NSE performance criteria: Implications for improving hydrological modelling, *Journal of Hydrology*, 377, 80–91, <https://doi.org/10.1016/j.jhydrol.2009.08.003>, <https://www.sciencedirect.com/science/article/pii/S0022169409004843>, 2009.
- Han, X., Hendricks Franssen, H.-J., Jiménez Bello, M. \., Rosolem, R., Bogen, H., Alzamora, F. M., Chanzy, A., and Vereecken, H.: Simultaneous soil moisture and properties estimation for a drip irrigated field by assimilating cosmic-ray neutron intensity, *Journal of Hydrology*, 580 539, 611–624, <https://doi.org/10.1016/j.jhydrol.2016.05.050>, <https://linkinghub.elsevier.com/retrieve/pii/S0022169416303171>, 2016.
- Hargreaves, G. H. and Samani, Z. A.: Reference Crop Evapotranspiration from Temperature, *Applied Engineering in Agriculture*, 1, 96–99, <https://doi.org/10.13031/2013.26773>, [http://ce.nmsu.edu/\\$sim\\$zsamani/papers/Hargreaves_Samani_85.pdf%5Cnhttp://elibrary.asabe.org/abstract.asp?JID=3&AID=26773&CID=aeaj1985&v=1&i=2&T=1](http://ce.nmsu.edu/simzsamani/papers/Hargreaves_Samani_85.pdf%5Cnhttp://elibrary.asabe.org/abstract.asp?JID=3&AID=26773&CID=aeaj1985&v=1&i=2&T=1), 1985.
- Hari, V., Rakovec, O., Markonis, Y., Hanel, M., and Kumar, R.: Increased future occurrences of the exceptional 2018–2019 Central 585 European drought under global warming, *Scientific Reports*, 10, <https://doi.org/10.1038/s41598-020-68872-9>, <https://doi.org/10.1038/s41598-020-68872-9>, ISBN: 4159802068872 Publisher: Nature Publishing Group UK, 2020.
- Hartmann, Jörg and Moosdorf, Nils: Global Lithological Map Database v1.0 (gridded to 0.5° spatial resolution), supplement to: Hartmann, Jens; Moosdorf, Nils (2012): The new global lithological map database GLiM: A representation of rock properties at the Earth surface. *Geochemistry, Geophysics, Geosystems*, 13, Q12004, <https://doi.org/10.1594/PANGAEA.788537>, [https://doi.pangaea.de/10.1594/](https://doi.pangaea.de/10.1594/PANGAEA.788537) 590 PANGAEA.788537, type: dataset, 2012.
- Itzerott, S., Hohmann, C., Stender, V., Maass, H., Borg, E., Renke, F., Jahncke, D., Berg, M., Conrad, C., and Spengler, D.: TERENO (North-east), Climate stations of the GFZ German Research Centre for Geosciences (GFZ), <https://doi.org/10.5880/TERENO.GFZ.CL.2018.ALL>, <http://dataservices.gfz-potsdam.de/tereno-new/showshort.php?id=escidoc:3508888>, type: dataset, 2018a.
- Itzerott, S., Hohmann, C., Stender, V., Maass, H., Borg, E., Renke, F., Jahncke, D., Berg, M., Conrad, C., and Spengler, D.: TERENO (Northeast), Soil moisture stations of the GFZ German Research Centre for Geosciences (GFZ), 595 <https://doi.org/10.5880/TERENO.GFZ.SM.2018.ALL>, <https://dataservices.gfz-potsdam.de/tereno-new/showshort.php?id=escidoc:3547898>, type: dataset, 2018b.
- Iwema, J., Rosolem, R., Rahman, M., Blyth, E., and Wagener, T.: Land surface model performance using cosmic-ray and point-scale soil moisture measurements for calibration, *Hydrology and Earth System Sciences*, 21, 2843–2861, [https://doi.org/10.5194/hess-21-2843-](https://doi.org/10.5194/hess-21-2843-2017) 600 2017, <https://hess.copernicus.org/articles/21/2843/2017/>, 2017.
- Kaspar, F., Müller-Westermeier, G., Penda, E., Mächel, H., Zimmermann, K., Kaiser-Weiss, A., and Deutschländer, T.: Monitoring of climate change in Germany – data, products and services of Germany’s National Climate Data Centre, *Advances in Science and Research*, 10, 99–106, <https://doi.org/10.5194/asr-10-99-2013>, <https://asr.copernicus.org/articles/10/99/2013/>, 2013.
- Keyantash, J. and Dracup, J.: The Quantification of Drought: An Evaluation of Drought Indices, *American Meteorological Society*, 2002.
- 605 Kiese, R., Fersch, B., Baessler, C., Brosy, C., Butterbach-Bahl, K., Chwala, C., Dannenmann, M., Fu, J., Gasche, R., Grote, R., Jahn, C., Klatt, J., Kunstmann, H., Mauder, M., Rödiger, T., Smiatek, G., Soltani, M., Steinbrecher, R., Völksch, I., Werhahn, J., Wolf, B., Zeeman, M., and Schmid, H.: The TERENO Pre-Alpine Observatory: Integrating Meteorological, Hydrological, and Biogeochemical Measurements and Modeling, *Vadose Zone Journal*, 17, 180 060, <https://doi.org/10.2136/vzj2018.03.0060>, <http://doi.wiley.com/10.2136/vzj2018.03.0060>, 2018.
- 610 Koster, R. D., Guo, Z., Yang, R., Dirmeyer, P. A., Mitchell, K., and Puma, M. J.: On the Nature of Soil Moisture in Land Surface Models, *Journal of Climate*, 22, 4322–4335, <https://doi.org/10.1175/2009JCLI2832.1>, <http://journals.ametsoc.org/doi/10.1175/2009JCLI2832.1>, 2009.

- Kumar, R., Samaniego, L., and Attinger, S.: Implications of distributed hydrologic model parameterization on water fluxes at multiple scales and locations: DISTRIBUTED HYDROLOGIC MODEL PARAMETERIZATIONS, *Water Resources Research*, 49, 360–379, <https://doi.org/10.1029/2012WR012195>, <http://doi.wiley.com/10.1029/2012WR012195>, 2013.
- Köhli, M., Schrön, M., Zreda, M., Schmidt, U., Dietrich, P., and Zacharias, S.: Footprint characteristics revised for field-scale soil moisture monitoring with cosmic-ray neutrons, *Water Resources Research*, 51, 5772–5790, <https://doi.org/10.1002/2015WR017169>, <https://agupubs.onlinelibrary.wiley.com/doi/abs/10.1002/2015WR017169>, 2015.
- Köhli, M., Weimar, J., Schrön, M., Baatz, R., and Schmidt, U.: Soil Moisture and Air Humidity Dependence of the Above-Ground Cosmic-Ray Neutron Intensity, *Frontiers in Water*, 2, <https://doi.org/10.3389/frwa.2020.544847>, <https://www.frontiersin.org/articles/10.3389/frwa.2020.544847/full>, 2021.
- Livneh, B., Kumar, R., and Samaniego, L.: Influence of soil textural properties on hydrologic fluxes in the Mississippi river basin: Influence of Soil Textural Properties on Hydrologic Fluxes, *Hydrological Processes*, 29, 4638–4655, <https://doi.org/10.1002/hyp.10601>, <http://doi.wiley.com/10.1002/hyp.10601>, 2015.
- Madruza de Brito, M., Kuhlicke, C., and Marx, A.: Near-real-time drought impact assessment: a text mining approach on the 2018/19 drought in Germany, *Environmental Research Letters*, 15, 1040a9, <https://doi.org/10.1088/1748-9326/aba4ca>, <https://iopscience.iop.org/article/10.1088/1748-9326/aba4ca>, 2020.
- Marx, A., Kumar, R., Thober, S., Rakovec, O., Wanders, N., Zink, M., Wood, E. F., Pan, M., Sheffield, J., and Samaniego, L.: Climate change alters low flows in Europe under global warming of 1.5, 2, and 3 °C, *Hydrology and Earth System Sciences*, 22, 1017–1032, <https://doi.org/10.5194/hess-22-1017-2018>, <https://hess.copernicus.org/articles/22/1017/2018/>, 2018.
- Mizukami, N., Clark, M. P., Newman, A. J., Wood, A. W., Gutmann, E. D., Nijssen, B., Rakovec, O., and Samaniego, L.: Towards seamless large-domain parameter estimation for hydrologic models: LARGE-DOMAIN MODEL PARAMETERS, *Water Resources Research*, 53, 8020–8040, <https://doi.org/10.1002/2017WR020401>, <http://doi.wiley.com/10.1002/2017WR020401>, 2017.
- Mo, K. C., Chen, L.-C., Shukla, S., Bohn, T. J., and Lettenmaier, D. P.: Uncertainties in North American Land Data Assimilation Systems over the Contiguous United States, *Journal of Hydrometeorology*, 13, 996–1009, <https://doi.org/10.1175/JHM-D-11-0132.1>, <http://journals.ametsoc.org/doi/10.1175/JHM-D-11-0132.1>, 2012.
- Pastorello, G., Trotta, C., Canfora, E., Chu, H., Christianson, D., Cheah, Y.-W., Poindexter, C., Chen, J., Elbashandy, A., Humphrey, M., Isaac, P., Polidori, D., Reichstein, M., Ribeca, A., van Ingen, C., Vuichard, N., Zhang, L., Amiro, B., Ammann, C., Arain, M. A., Ardö, J., Arkebauer, T., Arndt, S. K., Arriga, N., Aubinet, M., Aurela, M., Baldocchi, D., Barr, A., Beamesderfer, E., Marchesini, L. B., Bergeron, O., Beringer, J., Bernhofer, C., Berveiller, D., Billesbach, D., Black, T. A., Blanken, P. D., Bohrer, G., Boike, J., Bolstad, P. V., Bonal, D., Bonnefond, J.-M., Bowling, D. R., Bracho, R., Brodeur, J., Brümmer, C., Buchmann, N., Burban, B., Burns, S. P., Buysse, P., Cale, P., Cavagna, M., Cellier, P., Chen, S., Chini, I., Christensen, T. R., Cleverly, J., Collalti, A., Consalvo, C., Cook, B. D., Cook, D., Coursolle, C., Cremonese, E., Curtis, P. S., D’Andrea, E., da Rocha, H., Dai, X., Davis, K. J., Cinti, B. D., Grandcourt, A. d., Ligne, A. D., De Oliveira, R. C., Delpierre, N., Desai, A. R., Di Bella, C. M., Tommasi, P. d., Dolman, H., Domingo, F., Dong, G., Dore, S., Duce, P., Dufrêne, E., Dunn, A., Dušek, J., Eamus, D., Eichelmann, U., ElKhidir, H. A. M., Eugster, W., Ewenz, C. M., Ewers, B., Famulari, D., Fares, S., Feigenwinter, I., Feitz, A., Fensholt, R., Filippa, G., Fischer, M., Frank, J., Galvagno, M., Gharun, M., Gianelle, D., Gielen, B., Gioli, B., Gitelson, A., Goded, I., Goeckede, M., Goldstein, A. H., Gough, C. M., Goulden, M. L., Graf, A., Griebel, A., Gruening, C., Grünwald, T., Hammerle, A., Han, S., Han, X., Hansen, B. U., Hanson, C., Hatakka, J., He, Y., Hehn, M., Heinesch, B., Hinko-Najera, N., Hörtnagl, L., Hutley, L., Ibrom, A., Ikawa, H., Jackowicz-Korczynski, M., Janouš, D., Jans, W., Jassal, R., Jiang, S., Kato, T., Khomik, M., Klatt, J., Knohl, A., Knox, S., Kobayashi, H., Koerber, G., Kolle, O., Kosugi, Y., Kotani, A., Kowalski, A., Kruijt, B., Kurbatova, J., Kutsch,

- W. L., Kwon, H., Launiainen, S., Laurila, T., Law, B., Leuning, R., Li, Y., Liddell, M., Limousin, J.-M., Lion, M., Liska, A. J., Lohila, A., López-Ballesteros, A., López-Blanco, E., Loubet, B., Loustau, D., Lucas-Moffat, A., Lüers, J., Ma, S., Macfarlane, C., Magliulo, V., Maier, R., Mammarella, I., Manca, G., Marcolla, B., Margolis, H. A., Marras, S., Massman, W., Mastepanov, M., Matamala, R., Matthes, J. H., Mazzenga, F., McCaughey, H., McHugh, I., McMillan, A. M. S., Merbold, L., Meyer, W., Meyers, T., Miller, S. D., Minerbi, S.,
655 Moderow, U., Monson, R. K., Montagnani, L., Moore, C. E., Moors, E., Moreaux, V., Moureaux, C., Munger, J. W., Nakai, T., Neirynck, J., Nesic, Z., Nicolini, G., Noormets, A., Northwood, M., Nosetto, M., Nouvellon, Y., Novick, K., Oechel, W., Olesen, J. E., Ourcival, J.-M., Papuga, S. A., Parmentier, F.-J., Paul-Limoges, E., Pavelka, M., Peichl, M., Pendall, E., Phillips, R. P., Pilegaard, K., Pirk, N., Posse, G., Powell, T., Prasse, H., Prober, S. M., Rambal, S., Rannik, A., Raz-Yaseef, N., Rebmann, C., Reed, D., Dias, V. R. d., Restrepo-Coupe, N., Reverter, B. R., Roland, M., Sabbatini, S., Sachs, T., Saleska, S. R., Sánchez-Cañete, E. P., Sanchez-Mejia, Z. M., Schmid, H. P.,
660 Schmidt, M., Schneider, K., Schrader, F., Schroder, I., Scott, R. L., Sedláč, P., Serrano-Ortíz, P., Shao, C., Shi, P., Shironya, I., Siebicke, L., Šigut, L., Silberstein, R., Sirca, C., Spano, D., Steinbrecher, R., Stevens, R. M., Sturtevant, C., Suyker, A., Tagesson, T., Takanashi, S., Tang, Y., Tapper, N., Thom, J., Tomassucci, M., Tuovinen, J.-P., Urbanski, S., Valentini, R., van der Molen, M., van Gorsel, E., van Huissteden, K., Varlagin, A., Verfaillie, J., Vesala, T., Vincke, C., Vitale, D., Vygodskaya, N., Walker, J. P., Walter-Shea, E., Wang, H., Weber, R., Westermann, S., Wille, C., Wofsy, S., Wohlfahrt, G., Wolf, S., Woodgate, W., Li, Y., Zampedri, R., Zhang, J., Zhou, G., Zona, D.,
665 Agarwal, D., Biraud, S., Torn, M., and Papale, D.: The FLUXNET2015 dataset and the ONEFlux processing pipeline for eddy covariance data, *Scientific Data*, 7, 225, <https://doi.org/10.1038/s41597-020-0534-3>, <https://www.nature.com/articles/s41597-020-0534-3>, 2020.
- Peng, J., Albergel, C., Balenzano, A., Brocca, L., Cartus, O., Cosh, M. H., Crow, W. T., Dabrowska-Zielinska, K., Dadson, S., Davidson, M. W., de Rosnay, P., Dorigo, W., Gruber, A., Hagemann, S., Hirschi, M., Kerr, Y. H., Lovergine, F., Mahecha, M. D., Marzahn, P., Mattia, F., Musial, J. P., Preusmann, S., Reichle, R. H., Satalino, G., Silgram, M., van Bodegom, P. M., Verhoest, N. E., Wagner, W.,
670 Walker, J. P., Wegmüller, U., and Loew, A.: A roadmap for high-resolution satellite soil moisture applications – confronting product characteristics with user requirements, *Remote Sensing of Environment*, 252, 112 162, <https://doi.org/10.1016/j.rse.2020.112162>, <https://linkinghub.elsevier.com/retrieve/pii/S0034425720305356>, 2021.
- Pütz, T., Kiese, R., Wollschläger, U., Groh, J., Rupp, H., Zacharias, S., Priesack, E., Gerke, H. H., Gasche, R., Bens, O., Borg, E., Baessler, C., Kaiser, K., Herbrich, M., Munch, J.-C., Sommer, M., Vogel, H.-J., Vanderborght, J., and Vereecken, H.: TERENO-SOILCan: a lysimeter-
675 network in Germany observing soil processes and plant diversity influenced by climate change, *Environmental Earth Sciences*, 75, 1242, <https://doi.org/10.1007/s12665-016-6031-5>, <https://doi.org/10.1007/s12665-016-6031-5>, 2016.
- Rakovec, O., Kumar, R., Mai, J., Cuntz, M., Thober, S., Zink, M., Attinger, S., Schäfer, D., Schrön, M., and Samaniego, L.: Multiscale and Multivariate Evaluation of Water Fluxes and States over European River Basins, *Journal of Hydrometeorology*, <https://doi.org/10.1175/JHM-D-15-0054.1>, 2016.
- 680 Rakovec, O., Mizukami, N., Kumar, R., Newman, A. J., Thober, S., Wood, A. W., Clark, M. P., and Samaniego, L.: Diagnostic Evaluation of Large-Domain Hydrologic Models Calibrated Across the Contiguous United States, *Journal of Geophysical Research: Atmospheres*, 124, 13 991–14 007, <https://doi.org/10.1029/2019JD030767>, <https://onlinelibrary.wiley.com/doi/10.1029/2019JD030767>, 2019.
- Rakovec, O., Samaniego, L., Hari, V., Markonis, Y., Moravec, V., Thober, S., Hanel, M., and Kumar, R.: The 2018–2020 Multi-Year Drought Sets a New Benchmark in Europe, *Earth’s Future*, 10, <https://doi.org/10.1029/2021EF002394>, <https://onlinelibrary.wiley.com/doi/10.1029/2021EF002394>, 2022.
685
- Rauthe, M., Steiner, H., Riediger, U., Mazurkiewicz, A., and Gratzki, A.: A Central European precipitation climatology – Part I: Generation and validation of a high-resolution gridded daily data set (HYRAS), *Meteorologische Zeitschrift*, pp. 235–

- 256, <https://doi.org/10.1127/0941-2948/2013/0436>, https://www.schweizerbart.de/papers/metz/detail/22/81060/A_Central_European_precipitation_climatology_Part_?af=crossref, 2013.
- 690 Rosenbaum, U., Bogen, H. R., Herbst, M., Huisman, J. A., Peterson, T. J., Weuthen, A., Western, A. W., and Vereecken, H.: Seasonal and event dynamics of spatial soil moisture patterns at the small catchment scale: DYNAMICS OF CATCHMENT-SCALE SOIL MOISTURE PATTERNS, *Water Resources Research*, 48, <https://doi.org/10.1029/2011WR011518>, <http://doi.wiley.com/10.1029/2011WR011518>, 2012.
- Saha, T. R., Shrestha, P. K., Rakovec, O., Thober, S., and Samaniego, L.: A drought monitoring tool for South Asia, *Environmental Research Letters*, 16, 054 014, <https://doi.org/10.1088/1748-9326/abf525>, <https://iopscience.iop.org/article/10.1088/1748-9326/abf525>, 2021.
- 695 Samaniego, L., Kumar, R., and Attinger, S.: Multiscale parameter regionalization of a grid-based hydrologic model at the mesoscale: MULTISCALE PARAMETER REGIONALIZATION, *Water Resources Research*, 46, <https://doi.org/10.1029/2008WR007327>, <http://doi.wiley.com/10.1029/2008WR007327>, 2010.
- Samaniego, L., Kumar, R., and Zink, M.: Implications of parameter uncertainty on soil moisture drought analysis in Germany, *Journal of Hydrometeorology*, 14, 47–68, <https://doi.org/10.1175/JHM-D-12-075.1>, iISBN: 1525-755X, 2013.
- 700 Samaniego, L., Kumar, R., Thober, S., Rakovec, O., Zink, M., Wanders, N., Eisner, S., Müller Schmied, H., Sutanudjaja, E. H., Warrach-Sagi, K., and Attinger, S.: Toward seamless hydrologic predictions across spatial scales, *Hydrology and Earth System Sciences*, 21, 4323–4346, <https://doi.org/https://doi.org/10.5194/hess-21-4323-2017>, <https://hess.copernicus.org/articles/21/4323/2017/>, 2017.
- Samaniego, L., Thober, S., Kumar, R., Wanders, N., Rakovec, O., Pan, M., Zink, M., Sheffield, J., Wood, E. F., and Marx, A.: Anthropogenic warming exacerbates European soil moisture droughts, *Nature Climate Change*, 8, 421–426, <https://doi.org/10.1038/s41558-018-0138-5>, <https://www.nature.com/articles/s41558-018-0138-5>, 2018.
- Schattan, P., Baroni, G., Oswald, S. E., Schöber, J., Fey, C., Kormann, C., Huttenlau, M., and Achleitner, S.: Continuous monitoring of snow-pack dynamics in alpine terrain by aboveground neutron sensing: ALPINE SNOWPACK MONITORING BY CRNS, *Water Resources Research*, 53, 3615–3634, <https://doi.org/10.1002/2016WR020234>, <http://doi.wiley.com/10.1002/2016WR020234>, 2017.
- 710 Schrön, M., Köhli, M., Scheffele, L., Iwema, J., Bogen, H. R., Lv, L., Martini, E., Baroni, G., Rosolem, R., Weimar, J., Mai, J., Cuntz, M., Rebmann, C., Oswald, S. E., Dietrich, P., Schmidt, U., and Zacharias, S.: Improving calibration and validation of cosmic-ray neutron sensors in the light of spatial sensitivity, *Hydrology and Earth System Sciences*, 21, 5009–5030, <https://doi.org/https://doi.org/10.5194/hess-21-5009-2017>, <https://hess.copernicus.org/articles/21/5009/2017/>, 2017.
- Schrön, M., Zacharias, S., Womack, G., Köhli, M., Desilets, D., Oswald, S. E., Bumberger, J., Mollenhauer, H., Kögler, S., Remmler, P., Kasner, M., Denk, A., and Dietrich, P.: Intercomparison of cosmic-ray neutron sensors and water balance monitoring in an urban environment, *Geoscientific Instrumentation, Methods and Data Systems*, 7, 83–99, <https://doi.org/10.5194/gi-7-83-2018>, <https://gi.copernicus.org/articles/7/83/2018/>, 2018.
- 715 Sepulcre-Canto, G., Horion, S., Singleton, A., Carrao, H., and Vogt, J.: Development of a Combined Drought Indicator to detect agricultural drought in Europe, *Natural Hazards and Earth System Sciences*, 12, 3519–3531, <https://doi.org/10.5194/nhess-12-3519-2012>, <https://nhess.copernicus.org/articles/12/3519/2012/>, 2012.
- 720 Shuttleworth, J., Rosolem, R., Zreda, M., and Franz, T.: The COsmic-ray Soil Moisture Interaction Code (COSMIC) for use in data assimilation, *Hydrology and Earth System Sciences*, 17, 3205–3217, <https://doi.org/10.5194/hess-17-3205-2013>, <https://hess.copernicus.org/articles/17/3205/2013/>, 2013.

- Svoboda, M., LeComte, D., Hayes, M., Heim, R., Gleason, K., Angel, J., Rippey, B., Tinker, R., Palecki, M., Stooksbury, D.,
725 Miskus, D., and Stephens, S.: THE DROUGHT MONITOR, *Bulletin of the American Meteorological Society*, 83, 1181–1190,
<https://doi.org/10.1175/1520-0477-83.8.1181>, https://journals.ametsoc.org/view/journals/bams/83/8/1520-0477-83_8_1181.xml, 2002.
- Thober, S., Kumar, R., Sheffield, J., Mai, J., Schäfer, D., and Samaniego, L.: Seasonal Soil Moisture Drought Prediction over Europe Using
the North American Multi-Model Ensemble (NMME), *Journal of Hydrometeorology*, 16, 2329–2344, <https://doi.org/10.1175/JHM-D-15-0053.1>, <http://journals.ametsoc.org/doi/10.1175/JHM-D-15-0053.1>, 2015.
- 730 Tolson, B. A. and Shoemaker, C. A.: Dynamically dimensioned search algorithm for computationally efficient watershed model calibration,
Water Resources Research, 43, <https://doi.org/https://doi.org/10.1029/2005WR004723>, <https://agupubs.onlinelibrary.wiley.com/doi/abs/10.1029/2005WR004723>, 2007.
- USGS: Global Multi-resolution Terrain Elevation Data 2010 (GMTED2010), <https://doi.org/10.5066/F7J38R2N>, <https://www.usgs.gov/centers/eros/science/usgs-eros-archive-digital-elevation-global-multi-resolution-terrain-elevation>, type: dataset, 2017.
- 735 Vereecken, H., Huisman, J. A., Bogaen, H., Vanderborght, J., Vrugt, J. A., and Hopmans, J. W.: On the value of soil moisture
measurements in vadose zone hydrology: A review: SOIL MOISTURE AND HYDROLOGY, *Water Resources Research*, 44,
<https://doi.org/10.1029/2008WR006829>, <http://doi.wiley.com/10.1029/2008WR006829>, 2008.
- Wanders, N., Bierkens, M. F. P., de Jong, S. M., de Roo, A., and Karssenberg, D.: The benefits of using remotely sensed
soil moisture in parameter identification of large-scale hydrological models, *Water Resources Research*, 50, 6874–6891,
740 <https://doi.org/10.1002/2013WR014639>, <http://doi.wiley.com/10.1002/2013WR014639>, 2014.
- Western, A. W., Zhou, S.-L., Grayson, R. B., McMahon, T. A., Blöschl, G., and Wilson, D. J.: Spatial correlation of soil moisture
in small catchments and its relationship to dominant spatial hydrological processes, *Journal of Hydrology*, 286, 113–134,
<https://doi.org/10.1016/j.jhydrol.2003.09.014>, <https://linkinghub.elsevier.com/retrieve/pii/S0022169403003809>, 2004.
- Wiekenkamp, I., Huisman, J. A., Bogaen, H. R., and Vereecken, H.: Effects of Deforestation on Water Flow in the Vadose Zone, *Water*, 12,
745 35, <https://doi.org/10.3390/w12010035>, <https://www.mdpi.com/2073-4441/12/1/35>, 2019.
- Xia, Y., Sheffield, J., Ek, M. B., Dong, J., Chaney, N., Wei, H., Meng, J., and Wood, E. F.: Evaluation of multi-model simulated soil moisture in
NLDAS-2, *Journal of Hydrology*, 512, 107–125, <https://doi.org/10.1016/j.jhydrol.2014.02.027>, <http://dx.doi.org/10.1016/j.jhydrol.2014.02.027>, publisher: Elsevier B.V., 2014.
- Zacharias, S. and Wessolek, G.: Excluding Organic Matter Content from Pedotransfer Predictors of Soil Water Retention, *Soil Science
750 Society of America Journal*, 71, 43–50, <https://doi.org/10.2136/sssaj2006.0098>, <http://doi.wiley.com/10.2136/sssaj2006.0098>, 2007.
- Zacharias, S., Bogaen, H., Samaniego, L., Mauder, M., Fuß, R., Pütz, T., Frenzel, M., Schwank, M., Baessler, C., Butterbach-Bahl, K., Bens,
O., Borg, E., Brauer, A., Dietrich, P., Hajnsek, I., Helle, G., Kiese, R., Kunstmann, H., Klotz, S., Munch, J. C., Papen, H., Priesack, E.,
Schmid, H. P., Steinbrecher, R., Rosenbaum, U., Teutsch, G., and Vereecken, H.: A Network of Terrestrial Environmental Observatories
in Germany, *Vadose Zone Journal*, 10, 955–973, <https://doi.org/10.2136/vzj2010.0139>, <http://doi.wiley.com/10.2136/vzj2010.0139>, 2011.
- 755 Zink, M., Samaniego, L., Kumar, R., Thober, S., Mai, J., Schäfer, D., and Marx, A.: The German drought monitor, *Environmental Research
Letters*, 11, 074002, <https://doi.org/10.1088/1748-9326/11/7/074002>, <https://iopscience.iop.org/article/10.1088/1748-9326/11/7/074002>,
2016.
- Zink, M., Kumar, R., Cuntz, M., and Samaniego, L.: A high-resolution dataset of water fluxes and states for Germany accounting for
parametric uncertainty, *Hydrology and Earth System Sciences*, 21, 1769–1790, <https://doi.org/10.5194/hess-21-1769-2017>, ISBN: 1607-
760 7938, 2017.

Zreda, M., Shuttleworth, W. J., Zeng, X., Zweck, C., Desilets, D., Franz, T., and Rosolem, R.: COSMOS: the COsmic-ray Soil Moisture Observing System, *Hydrology and Earth System Sciences*, 16, 4079–4099, <https://doi.org/https://doi.org/10.5194/hess-16-4079-2012>, <https://hess.copernicus.org/articles/16/4079/2012/>, 2012.